Numerical Analysis of Flow Phenomena in a Centrifugal Pump of Low Specific Speed

By

Muhammad Ali
Reg # 00000205966
Session 2017-2019

Supervised by
Dr. Adeel Javed

A Thesis Submitted to the US Pakistan Centre for Advanced Studies in Energy in partial fulfillment of the requirements of the degree of

MASTER of SCIENCE
in
THERMAL ENERGY ENGINEERING

US-Pakistan Centre for Advanced Studies in Energy
(USPCAS-E)
National University of Sciences and Technology (NUST) H-12,
Islamabad 44000, Pakistan

March 2020

THESIS ACCEPTANCE CERTIFICATE

Certified that final copy of MS/MPhil thesis written by Mr. Muhammad Ali, (Registration No. 00000205966), of U.S.-Pak Centers for Advance Studies in Energy has been vetted by undersigned, found complete in all respects as per NUST Statues/Regulations, is within similarities indices limit and accepted as partial fulfillment for award of MS/MPhil degree. It is further certified that necessary amendments as pointed out by GEC members of the scholar have also been incorporated in the said thesis.

Signature: _____

Name of Supervisor: Dr. Adeel Javed

Date: _____

Signature (HoD): _____

Date: _____

Signature (Dean/Principal): _____

Date: _____

Certificate

This is to certify that work in this thesis has been carried out by **Mr. Muhammad Ali** and completed under my supervision in, U.S.-Pak Centers for Advance Studies in Energy, National University of Sciences and Technology, H-12, Islamabad, Pakistan.

Supervisor: _____

Dr. Adeel Javed
U.S.-Pak Centers for Advance Studies in Energy
NUST, Islamabad

GEC member 1: _____

Dr. Majid Ali
U.S.-Pak Centers for Advance Studies in Energy
NUST, Islamabad

GEC member 2: _____

Dr. Adeel Waqas
U.S.-Pak Centers for Advance Studies in Energy
NUST, Islamabad

GEC member 3: _____

Dr. Mariam Mahmood
U.S.-Pak Centers for Advance Studies in Energy
NUST, Islamabad

HoD-TEE: _____

Dr. Adeel Javed
U.S.-Pak Centers for Advance Studies in Energy
NUST, Islamabad

A/Principal: _____

Dr. Adeel Waqas
U.S.-Pak Centers for Advance Studies in Energy
NUST, Islamabad

Acknowledgment

I am extremely thankful to Allah Almighty without Whose help I would not have been able to complete this work. All the help and support from my parents and teachers were only because of Allah's Will.

I am thankful to my supervisor, Dr. Adeel Javed, for the tremendous supervision, motivation and guidance he has conveyed all through my time as his understudy. I have been exceptionally honored to have a supervisor who thought such a great amount about my work, and who responded to my inquiries and questions so immediately.

I am thankful to HoD Research Dr. Majid Ali, all GEC members, USPCAS-E and Golden Pumps Pvt. Limited for their provision all over the program.

Finally, I am grateful for the National University of Sciences and Technology, Pakistan and Oregon State University, USA for providing research facilities in my work.

Dedicated to my beloved parents and all educated community who lead me to such tremendous and wonderful accomplishment and success

Abstract

The computational fluid dynamics (CFD) analysis of a low specific speed centrifugal pump has been done. This work aims to improve the hydraulic performance of centrifugal pump defined as efficiency and cavitation. The shear stress transport (SST) k-ω turbulence model which is RANS based model is employed for 3-D steady state analysis using Ansys CFX. In the first part, the performance of impeller is moderately improved with the parametric analysis of two design parameters: blade wrap angle and outlet blade angle. The large wrap angle of the impeller blades reduces the shaft power consumption and large outlet angle increases the head of pump marginally. In the second part, the two different volutes with radial and tangential diffusers are analyzed. The volute with tangential diffuser shifted the design condition towards higher flow rate with the efficiency rise of 8.5% as compared to the baseline volute with radial diffuser. In the third part, Rayleigh-Plesset model is used to investigate the two-phase cavitating flow. The inlet blade angle is chosen as a design parameter to improve the cavitation performance of the pump. The blade inlet angle affects the suction capability of the pump and therefore affects the cavitating condition of the pump. The inlet angle of 18˚ enhanced the cavitation performance giving NPSH of 1.12 m decline as compared to the baseline pump.

Keywords: centrifugal pump, specific speed, CFD, design parameters, efficiency, cavitation

Table of Contents

List of Figures

Nomenclature

Variables	
c	absolute velocity
c_θ	circumferential or tangential velocity
Fr	radial force
H	Head
LE	leading edge of blade
N	rotational speed
N_q	specific speed
P_s	shaft power
p	static pressure
p_v	vapor pressure
Q_d	design flow rate
Re	Reynolds number
TE	trailing edge of blade
T	torque
u_2	blade tip velocity
w	relative velocity
y^+	dimensionless distance from the wall
ω	rotation speed
η_h	hydraulic efficiency
β	blade angle
ϕ	blade wrap angle
Abbreviations	
BEP	best efficiency point
NPSH	net positive suction head
CFD	Computational Fluid Dynamics

Chapter 1

Introduction

1.1 Background

Centrifugal pumps are commonly used in industries, irrigation and other domestic applications consuming large amount of electrical energy. Therefore, extensive research has been done to improve the optimized design of centrifugal pumps which greatly contributes to energy conservation. For each point of efficiency rise, this can save a huge amount of energy during the whole service life of pumps. The design of centrifugal pumps based on 1-dimensional theory uses the steady-state condition, empirical data and design experiences. Pump design methods recommended by Stepanoff, Pfleiderer, Newman and Gulich are widely accepted by pump manufacturers. However, the detailed analysis of the complex flow inside the pump is still required for optimum design.

The flow inside a centrifugal pump is 3-dimensional, turbulent and unsteady with secondary flow losses and flow recirculation. The performance of the pump deteriorates at off-design conditions and can severely reduce the life of pumps.

1.2 Literature Review

The first approach for the optimization design is to use traditional one-dimensional design theory and now it has been advanced to three-dimensional design method. Inverse design method proposed by Gulich [1] is widely used by pump designers which gives the optimal geometry of the pump by defining the design conditions i.e. flow rate, head, and rpm. Another approach is to optimally combine design variables like blade angles, meridional shape etc. Xu et al. [2] in his research used CFD tools to find the combination of design parameters by orthogonal method for optimal design of the impeller. Yuan et al. [3] investigated the flow instabilities caused by cavitation through experimental means. Donmez et al. [4] presented how cavitation can be resisted by varying blade inlet angles on inner and outer streamline of blades. Tan et al. [5] examined the effect of blade wrap angle on performance of centrifugal pump and verified it with experimental setup. Outlet blade angles and wrap angle are significant parameters in optimization design of impeller

[6], [7]. Kim et al. [8] reduced the flow recirculation and cavitation using multiple design variables such as meridional profile and incidence angles. Cheah et al. [9] investigated the unsteady flow with pressure variations and unstable operation. The flow analysis of the volute of centrifugal pump with low specific speed is studied by Keldar et al. [10]. Alemi et al. [11] developed new multi-volute shape for radial thrust reductions in centrifugal pumps.

Weidong et al. [12] studied the influence of impeller eccentricity on centrifugal pump. Fei Zhao et al. [13] developed orthogonal method to optimize the impeller design. Combes et al. [14] numerically studied the unsteady radial thrust in centrifugal pump. Zangeneh et al. [15] developed a guideline for the design of centrifugal impellers with suppressed secondary flows. Pedersen et al. [16] investigated the performance of pump impeller at various operating conditions using Large Eddy Simulations (LES). Luo et al. [17] investigated the unstable operation of centrifugal pumps using MPANS model. Zhao et al. [18] improved the meridional shape optimization of centrifugal pumps.. Lettieri et al. [19] investigated non-linear flow variations in high pressure pumps. Benturki et al. [20] enhanced the efficiency and suction capability of centrifugal pump improvising NASA-II algorithm.

Friedrichs et al. [21] experimentally studied the rotating cavitation in centrifugal pump impeller by high speed camera techniques. Li et al. [22] found that pre-rotation in inlet of impeller causes unsteady flow in the pump operating at part-load conditions. Magagnato et al. [23] described the flow simulation in centrifugal pump using harmonic balance method as faster method compared to other simulation techniques. Yang et al. [24] studied the effects of volute curvature to improve the pump performance. Alemi et al. [25] designed the spiral volute and analyzed the effects on the performance of low specific speed pump operating at range of flow rates. Torabi et al. [26] presented vigorous hydrodynamic design of volute to reduce the radial forces when pump operates at part-load conditions. Spence at al. [27] studied the time varying pressure pulsations using transient CFD simulations. Most of the studies take into account the optimization of radial impeller by changing blade outlet angle and wrap angle [28], [29]. Grietzer [30] reviewed

all types of instabilities which are encountered in pumping systems. Wiesner [31] reviewed different methodologies for the estimation of slip phenomena for centrifugal pump impellers. Breugelmans [32] analyzed the effects of flow recirculation in the centrifugal pump. Bradshaw et al. [33] investigated the influence of impeller suction specific speed on vibration performance of centrifugal pump. Schiavello [34] discussed various NPSH criteria, pump cavitation and impeller life expectancy. Hirschi et al. [35] discussed the deterioration of pump performance due to cavitation appearing at leading edge of the blades. Franz et al. [36] examined the excitation forces generated by cavitating flow in the pumps. Bonaiuti et al. [37] presented multi-objective optimization technique of turbomachinery blade design. Lorett et al. [38] critically analyzed the flow deviation from impeller to volute at all operating points.

Computational fluid dynamics (CFD) is widely used in to investigate the flow through turbomachines and helps in improvement of design methodology with significantly low cost and less time. Unfortunately, domestic pump manufacturers in Pakistan are not using this methodology to design centrifugal pump.

1.3 Objectives

This work aims to analyze the steady, 3-dimensional flow phenomena in a centrifugal pump with low specific speed by computational fluid dynamics (CFD).

1. Extracting performance data of baseline centrifugal pump
2. Multi-objective performance enhancement design in terms of

a) Efficiency

b) Cavitation - Net positive suction head (NPSH)

3. To reduce hydraulic losses in impeller and volute of centrifugal pump
4. Recommending the suitable design parameters of impeller and volute

This will help in analyzing the flow losses in various components of the pump. The optimum combination of design parameters of impeller and volute can significantly

reduce the flow losses which will ultimately improves the hydraulic performance of the centrifugal pump. The methodology to improve the performance of centrifugal pump in terms of efficiency and cavitation is shown in Fig 1.1.

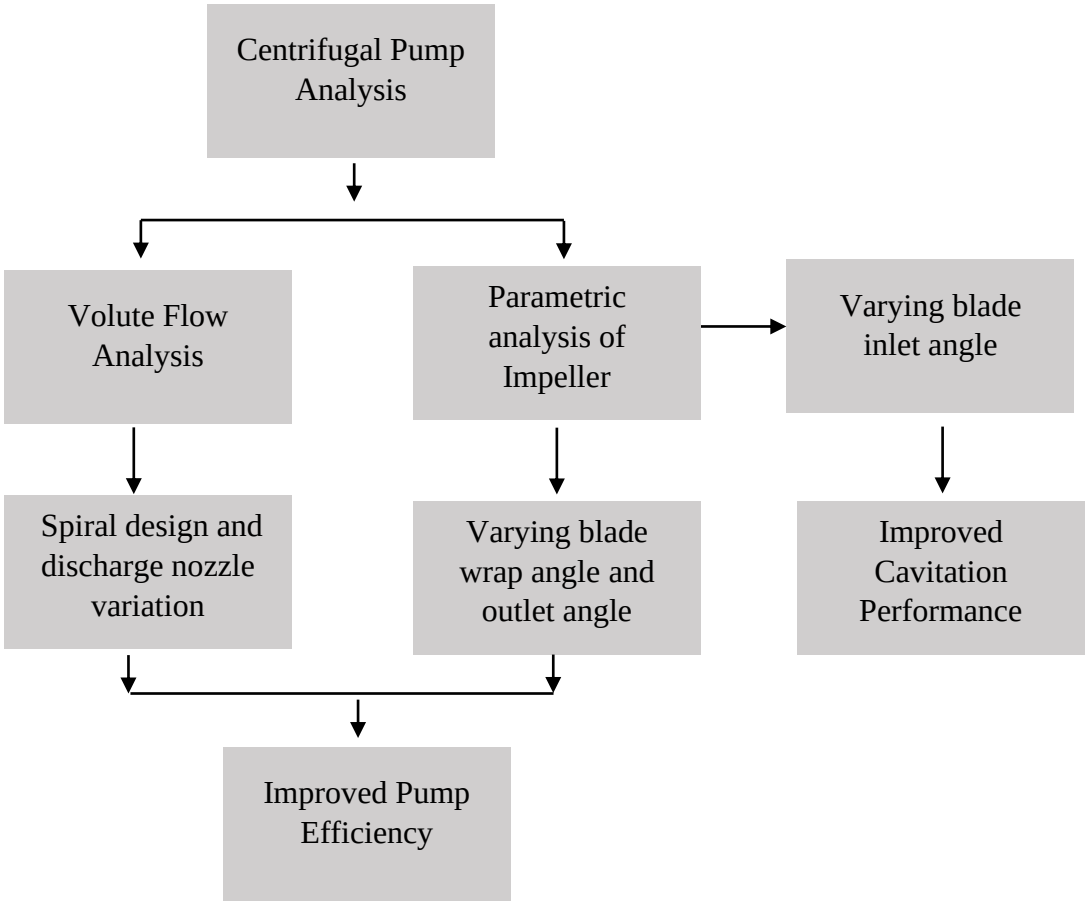

Figure 1.1 Methodology for flow analysis of impeller and volute of centrifugal pump

1.4 Thesis Outline

The following is a summary of the different chapters in this thesis.

Chapter 2 describes the turbulence model used in the simulation and computational grid of the centrifugal pump components. In addition, boundary conditions are described for both cavitating and non-cavitating conditions as well.

Chapter 3 discusses the flow characteristics inside the impeller. The effect of two design parameters, wrap angle and blade outlet angle, on the secondary flow losses is investigated. The performance of the impeller is improved by the best combination of design variables.

Chapter 4 describes the centrifugal pump model with impeller, volute and suction/discharge pipes are simulated. The volute design methodologies and the volutes with radial and tangential discharge nozzles are discussed.

Chapter 5 shows the two-phase flow simulations due to cavitation. The NPSH of baseline pump is improved by the variation of inlet blade angle to control inflow conditions.

Chapter 6 contains the conclusions and future recommendations to continue this research work.

Chapter 7 describes the brief research work carried out in thermal energy lab of Oregon State University USA.

Appendices The mathematical model of all the necessary calculations are given in appendix A. In addition, the impeller design code (1-D) is also developed in Engineering Equation Solver (EES) from the pump design reference Gulich [1] given in appendix B.

Chapter 2

Numerical Method

2.1 Centrifugal Pump Model

The pump model used in this project is a single stage centrifugal pump manufactured by Golden Pumps Pvt. Limited. The specifications of the pump are given in Table 2.1. The impeller is drawn in BladeGen ANSYS by defining the meridional shape, blade angles and thickness. The volute is designed in CFTurbo by defining the volute rotation start angle, inlet width, spiral outlet radius and cutwater position. The entire computational domain consists of suction pipe, impeller, volute and discharge pipe shown in Fig. 2.2. The computational domain does not include the fluid in the impeller and casing gaps. The roughness of the material is not considered in the simulations and frictional losses will only be due to the viscosity of fluid.

Specific speed is used to classify impellers on the basis of their performance regardless of size and speed at which it operates.

$$Specific\ speed = N_q = N\frac{\sqrt{Q}}{H^{3/4}} \tag{2.1}$$

The pump is identified by the capacity, head and rotational speed. These parameters are inter-related by specific speed which determines the impeller type and design. Specific speed is also used in choosing the pump type i.e. radial, mixed or axial flow depending upon the application of pump. The small size pumps as in this case should be of low specific speed considering the economic limit and performance of the pump.

The meridional shape of impeller blades having low specific speed is purely radial and having no sweep and lean at leading and trailing edge of blades. The hub and shroud angles at any position of the blades are same. The bade angles at inlet and outlet are obtained by circular arc as shown in Fig. 2.1.

Table 2.1. Geometric parameters of the test pump

Description	**Parameter**	**Value**
Design flow rate	$Q/(m^3.h^{-1})$	3.6
Head	$H/(m)$	18
Rotation speed	$N/(rev.min^{-1})$	2900
Specific speed	N_q	10.5
Number of blades	Z	6
Impeller inlet diameter	$D_1/(mm)$	42
Impeller outlet diameter	$D_1/(mm)$	130
Inlet blade angle	$\beta_1/(°)$	26
Outlet blade angle	$\beta_2/(°)$	36.5
Blade wrap angle	$\varphi/(°)$	82

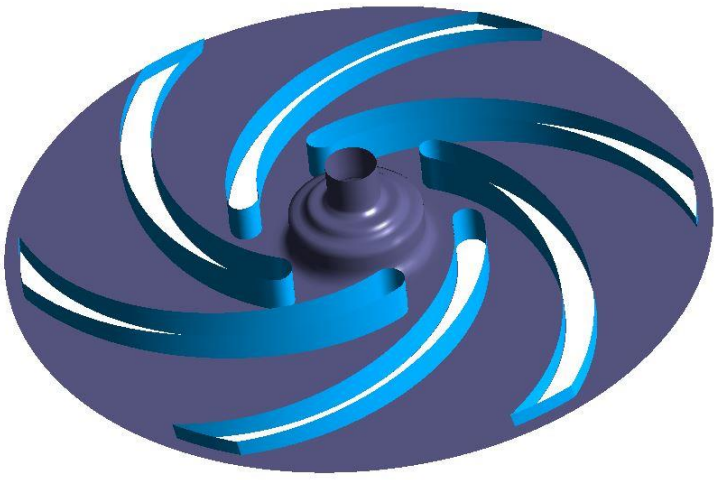

Figure 2.1 Isometric view of the impeller

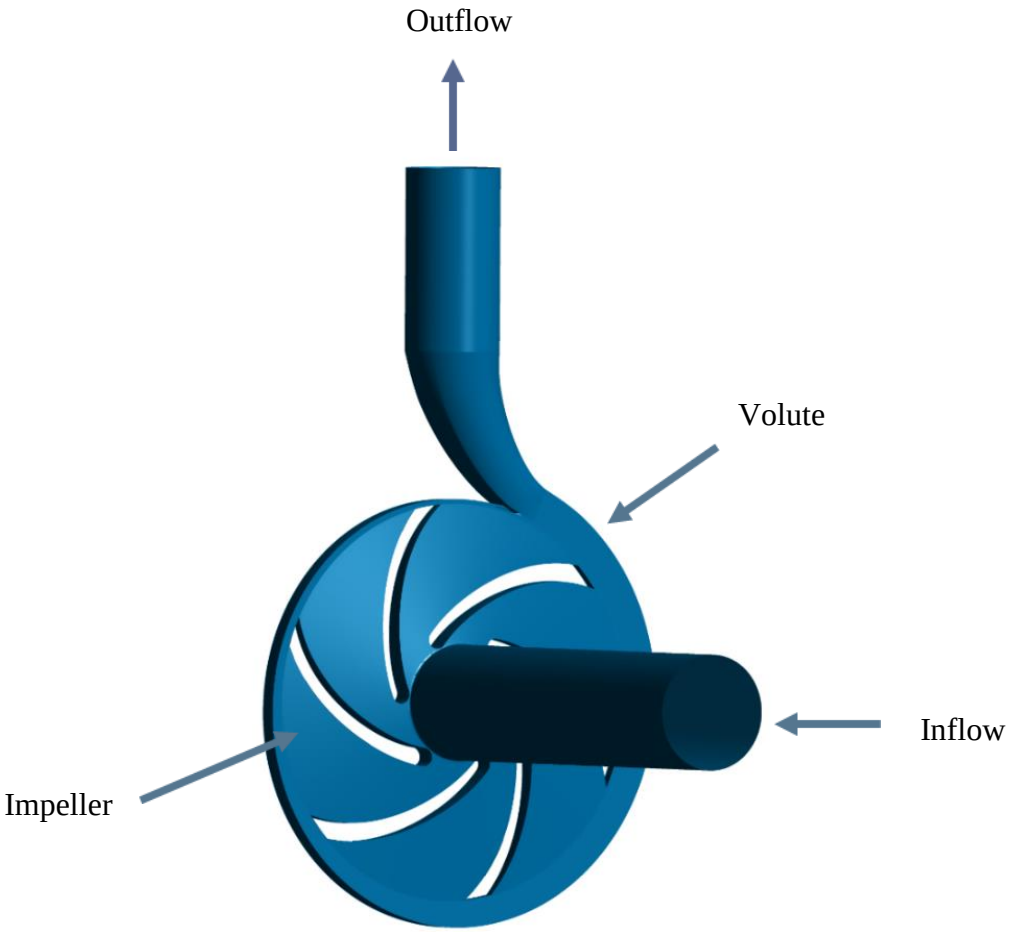

Figure 2.2 3-D model of the computational

2.2 Reynolds Averaged Navier-Stokes (RANS) equations

The multiple frame of reference i.e. stationary and rotating are used, and the equations must be organized in both frame of references. For three-dimensional incompressible steady flow, the continuity and momentum equation can be written as follows:

$$\frac{\partial u_i}{\partial x_i} = 0 \tag{2.2}$$

$$\rho \frac{\partial}{\partial x_i}\left(\overline{u_i u_j}\right) = -\frac{\partial \overline{P}}{\partial x_i} + \frac{\partial}{\partial x_j}\left(\overline{\tau_{ij}} - \rho\overline{u_i u_j}\right) + S_{u_i} \tag{2.3}$$

where

$$\vec{S}_{u_i} = -\rho\left[2\vec{\Omega} \times \vec{u} + \vec{\Omega} \times (\vec{\Omega} \times \vec{r})\right] \tag{2.4}$$

$$\overline{\tau_{ij}} = -\mu\left(\frac{\partial u_i}{\partial x_j} + \frac{\partial u_j}{\partial x_j}\right) \tag{2.5}$$

2.3 Shear Stress Transport (SST) turbulence model

Numerical calculations are done using CFX which solve 3-D Reynolds Averaged Navier-Stokes (RANS) equations for steady incompressible flow [39]. The SST (shear stress transport) turbulence model [40] is adopted which employs k-ω model close to the wall surface and k-ε model in the passage flow.

2.4 Cavitation Model

The two-phase (vapor-liquid) flow occur inside the pump when the fluid's static pressure falls below its saturation pressure. The model established on Rayleigh-Plesset equations is used to examine the cavitating (two-phase) flow. This model executed in CFX involves the nuclei radius which is assumed to be 1µm. The two-phase flow is considered as a homogeneous mixture having the same flow conditions. At inflow condition, vapor volume fraction is assigned a zero value because vapors will generate within the impeller as cavitation starts. The total pressure is lowered step-by-step at inlet while keeping mass flow rate fixed at the outlet.

2.5 Computational Grids

The structured mesh (hexahedral) elements of the impeller are generated in Turbo-Grid shown in Fig. 2.3. The mesh is carefully refined to satisfy the requirement of y^+value which is the dimensionless distance from the walls. $y^+ < 1$ is maintained at the wall surface of hub, shroud and blade except the trailing edge to investigate flow in viscous sublayer.

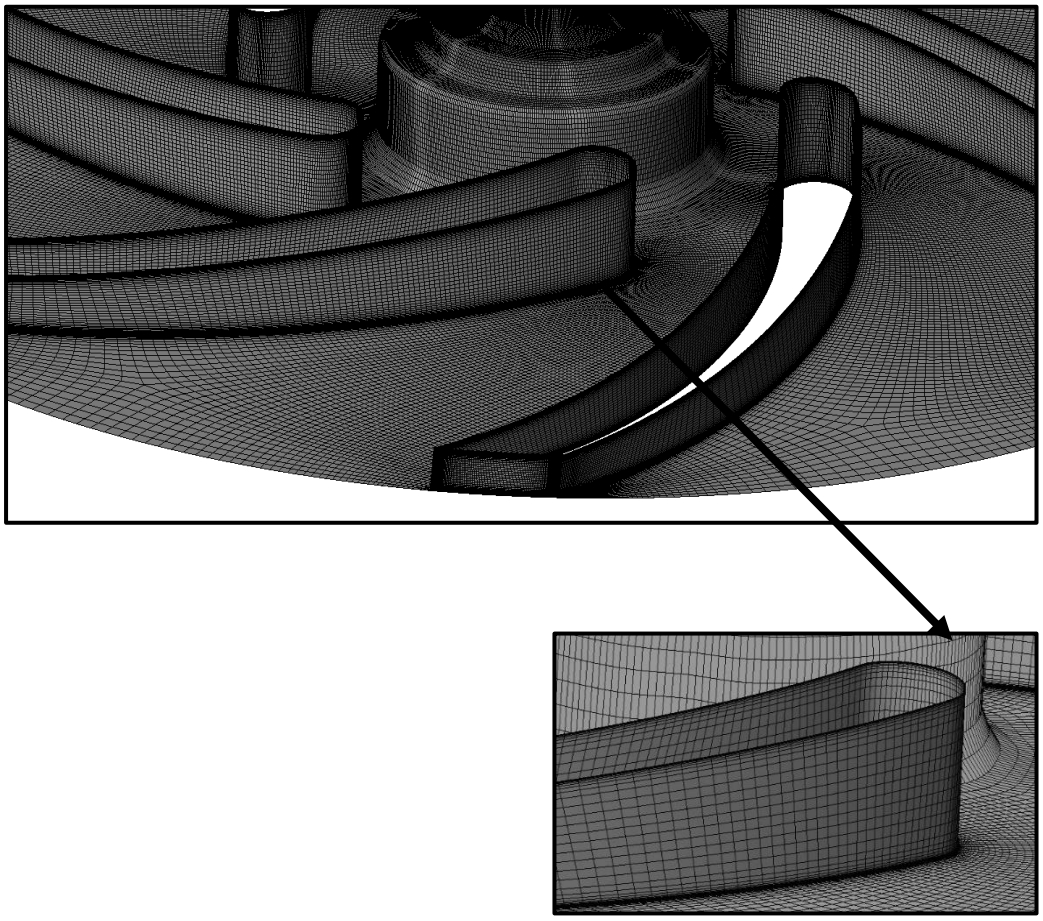

(a) Mesh of the impeller with refined leading

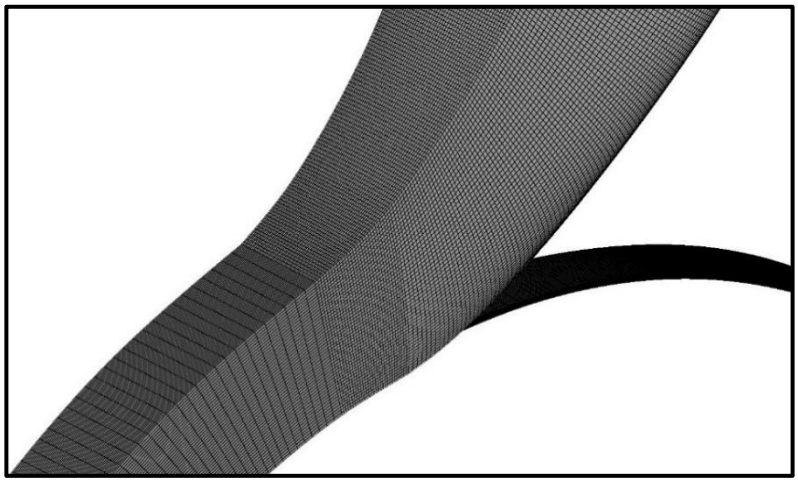

(b) Mesh of the volute

Figure 2.3 Computational domain of the model centrifugal pump

The mesh elements may affect the CFD results, that's why grid independence test is carried out. Five meshes of impeller are created varying from coarse to the finer grid. As the mesh reaches 1,20,000 elements, the head does not change significantly as shown in Fig. 2.4. Therefore, 1,20,000 mesh elements for a single passage is chosen in numerical simulations of the model impeller.

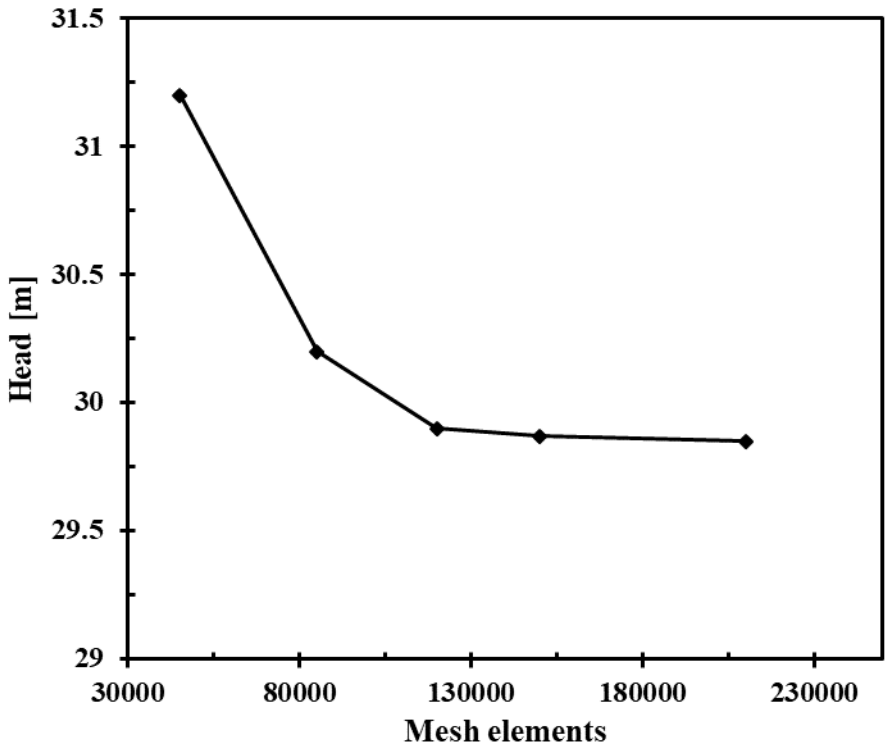

Figure 2.4 Mesh independence study

Structured mesh elements for the rectangular cross-section volute and inlet, outlet pipes are also generated in Pointwise. Mesh elements of volute and inlet pipes are 1,503,026 and 141,659 respectively. These elements were fixed in the mesh independence study.

2.6 Boundary Conditions

The impeller blade and surfaces of hub and shroud are solid boundaries (smooth walls) for the fluid flow subject to no-slip boundary conditions. Water at standard ambient

conditions (25℃) is used as a working fluid. The inlet boundary condition is defined by total pressure and mass flow rate is set at the outlet. Operating the pump at various flow rates, the pump performance curves are obtained.

2.7 Steady Flow Analysis

The steady flow analysis has been done in this work with stationary and rotating zone because the flow in impeller is in rotating frame of reference and flow in volute casing and suction/discharge pipes are in stationary frame. The intake pipe, impeller and volute are connected by means of a 'Frozen-Rotor' interface. The numerical computation is considered converged when the maximum residual 10^{-4} is reached.

Chapter 3

Flow Analysis of Centrifugal Impeller

In this chapter, the impeller is simulated at various flow rates to analyze its performance. The head curve of the impeller follows the trendline of test data as shown in Fig. 3.1 (a). The CFD results cannot be compared in the values with the test data as the computational domain contain consist of impeller only. Fig. 3.1 (b) shows the efficiency and shat power requirement of the impeller. The performance curve shows the best efficiency point achieves at $3.6 m^3/h$. As can be seen, the impeller efficiency is already operating at 95% efficiency at the design point, there is very little margin of improvement in its performance. The velocity contours at part load condition, design condition and high flow rate are analyzed to identify the secondary flow regions inside the impeller.

Centrifugal pump performance is described by plotting the head at various flow rates. A characteristic curve also includes its hydraulic efficiency and shaft power for various flow rates.

The suction head of pump is given as

$$h_1 = z_1 + \frac{p_1}{\rho g} + \frac{u_1^2}{2g} \tag{3.1}$$

and discharge head is

$$h_2 = z_2 + \frac{p_2}{\rho g} + \frac{u_2^2}{2g} \tag{3.2}$$

Where z_1 and z_2 are the elevation head at suction and discharge with respect to pump centerline and $u_1$and u_2 is the velocity of fluid at suction and discharge respectively.

The pump dynamic head is the difference of discharge and suction head

$$H = z_2 - z_1 + \frac{p_2 - p_1}{\rho g} + \frac{u_2^2 - u_1^2}{2g} \tag{3.3}$$

Most of the cases, $u_1 \approx u_2$ and $z_1 \approx z_2$, therefore the total head is equal to the difference between pressure head at discharge and intake of the pump.

$$H = \frac{p_{tot_{outlet}} - p_{tot_{inlet}}}{\rho_{water} \times g} \tag{3.4}$$

The efficiency of the centrifugal pump is calculated on the basis of shaft power, flow rate and total pump head

$$\eta_{hyd} = \frac{\rho g Q H}{T.\omega} \tag{3.5}$$

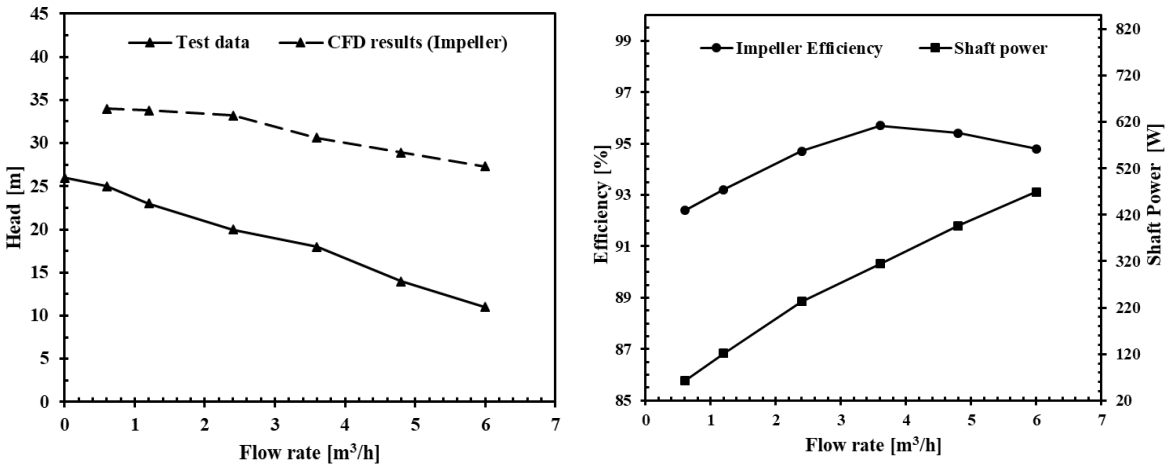

(a) Q-H curves (b) Efficiency and shaft power

Figure 3.1 Performance curves of the pump impeller

3.1 Selection of Design Variables

The important step is to choose the design parameters for optimization. The model pump impeller blades were in cylindrical form (untwisted blades) i.e. the shape of the blade is defined by a circular arc. Therefore, blade angles at hub and shroud and meridional shape

could not be varied. According to Euler's turbomachine equation, the theoretical head of centrifugal pump is defined by

$$H_{th} = \frac{1}{g}(u_2 c_{\theta 2} - u_1 c_{\theta 1}) \tag{3.6}$$

where $c_{\theta 2}$ and $c_{\theta 1}$ are circumferential velocity of the fluid at impeller outlet and inlet respectively which are linked with blade angles. With fixed impeller diameter and rpm, the outlet blade angle has great impact on the head of pump. Therefore, outlet blade angle is chosen as optimization design parameter. The blade wrap angle is also selected as design parameter which controls the flow path.

3.2 Effect of Varying Blade Wrap Angle

The angle made by the tangent lines on leading and trailing edge of the blade defines the blade wrap angle. The wrap angle is varied from 65º to 110º. A large wrap angle offers controlled flow in the impeller by reducing the secondary losses (flow separation). But as the wrap angle increases, the fluid has to undergo long flow path and produce more friction losses. A small wrap angle generates short flow path with less frictional losses, but the flow distribution is not uniform and higher secondary losses will occur. The relative velocity contours on mid-span location of the impeller with different wrap angles are shown in Fig. 3.2. The comparison of shaft power consumption at various flow rates is shown in Fig. 3.3. In terms of hydraulic performance, the impeller with wrap angle 110º offers relatively higher efficiency by reducing the shaft power consumption with marginal loss in the head (due to higher frictional losses) shown in Fig. 3.4.

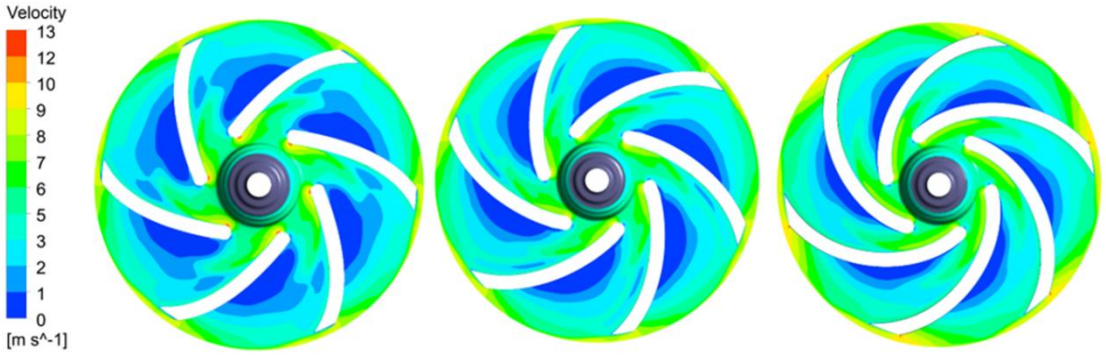

(a) Wrap 65º (b) Wrap 82º (c) Wrap 110º

Figure 3.2 Relative velocity contours at mid-span of impeller for different wrap angles

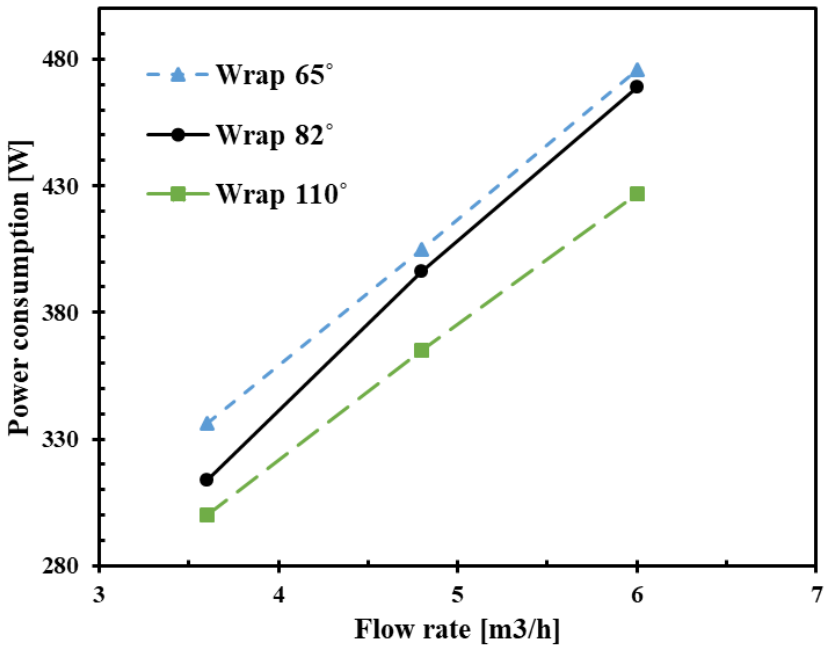

Figure 3.3 Comparison of shaft power consumption for different wrap angles

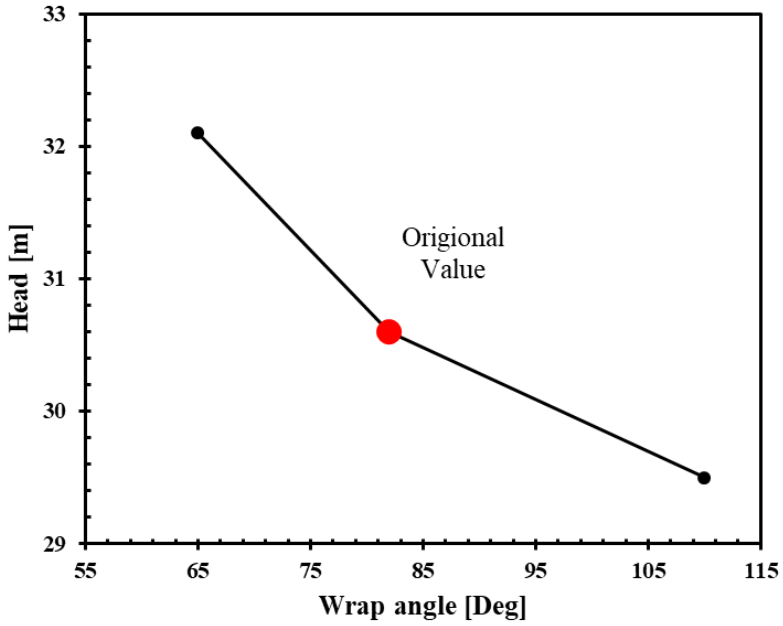

Figure 3.4 Variation of head at different wrap angles

3.3 Effect of Varying Blade Outlet Angle

The blade outlet angle is varied from 22º to 50º to get its impact on head and efficiency of the pump. The impeller with wrap angle of 110º has been simulated with varying outlet blade angle. It can be seen from velocity triangle at impeller outlet in Fig. 3.5, $c_{\theta 2}$ increases with large outlet angle which is transferred to the fluid in the form of head.

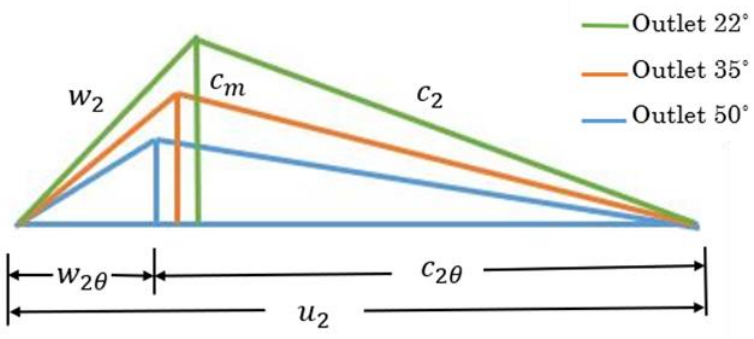

Figure 3.5 Velocity triangles at different blade outlet

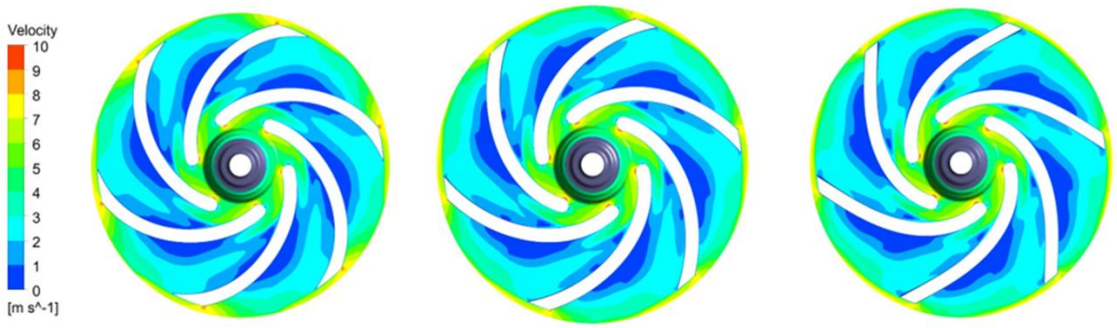

(a) Outlet 22º (b) Outlet 36º (c) Outlet 50º

Figure 3.6 Relative velocity contours at mid-span of impeller for different blade outlet

The relative velocity contours for different outlet angles are shown in Fig. 3.6. The boundary layer (separation losses) minimize on suction side of the blades with increasing outlet angle. With increase of outlet blade angle, head continuously increases as shown in Fig. 3.7.

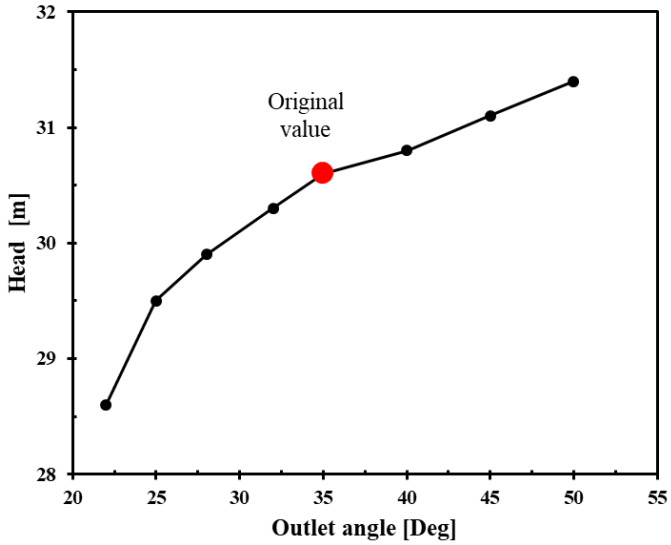

Figure 3.7 Variation of head at different blade outlet angles

3.4 Performance Comparison of Optimal Impeller

By choosing the best design parameters of wrap angle 110º and blade outlet angle 50º, the efficiency of the impeller is marginally improved by increasing the head and lowering the shaft power consumption. The comparison in the performance of optimal and original impeller are shown in Figs. 3.8 (a) and (b).

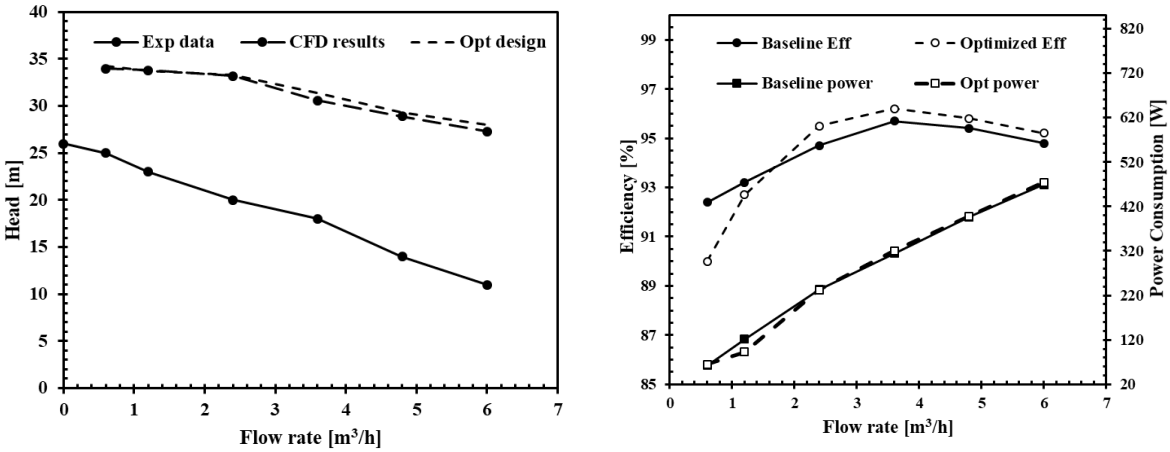

(a) Q-H curves

(b) Efficiency and Shaft power

Figure 3.8 Comparison of the performance of the original and optimal impeller

Summary

In this chapter, the flow inside the impeller is investigated and the performance curves are extracted at various flow rates. The design parameters namely the blade wrap angle and blade outlet angle are varied to analyze its effect on the performance of the impeller. The impeller with blade wrap angle 110º and outlet angle 50º produces a relatively better flow in the impeller with 0.8m rise in head and 0.6% increase in efficiency.

Chapter 4

Flow Analysis of Volute Casing

In this chapter, the flow in the pump is simulated with inlet pipe, impeller, volute casing and outlet pipe. The full impeller is used in the computational domain because of the asymmetrical volute outside the impeller as shown in Fig. 4.1. The inlet and outlet pipe with appropriate lengths are used in the simulation to reduce the effect of boundary conditions due to recirculation at inlet and outlet.

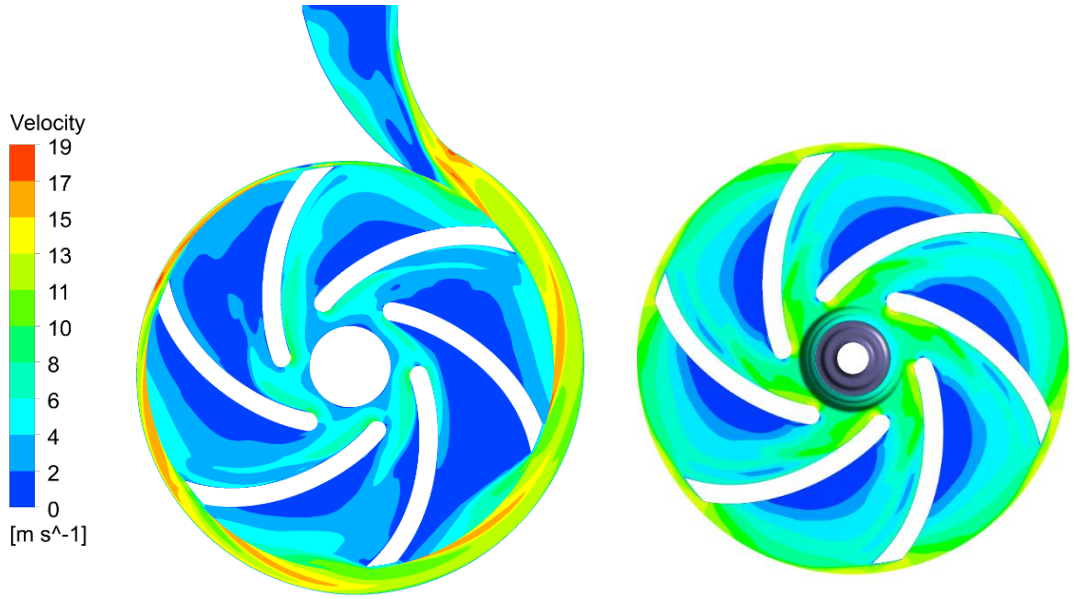

(a) with asymmetrical volute (b) without volute

Figure 4.1 Relative velocity contours in pump with and without volute

The CFD results show that the pump head is close to the test data at low flow rates (part-load operation) but deviates largely at higher flow rates. The main reason for high error in the values at higher flow rates is the shaft power requirement. According to Golden Pumps data, the pump is driven by 0.5 hp (370 W) induction motor. Fig. 4.2 (b) shows that at BEP (best efficiency point) and above, power requirement increases from 315W to 470W,

therefore, the predicted head is higher than baseline head. Also, the impeller sidewall gaps are not included in the computational domain in which flow leakage occurs that further produces the head loss. The performance curves of the centrifugal pump are shown in Figs. 4.2 (a) and (b). The pump has efficiency of 69% at BEP and this shows that secondary losses are higher in the volute as compared to impeller.

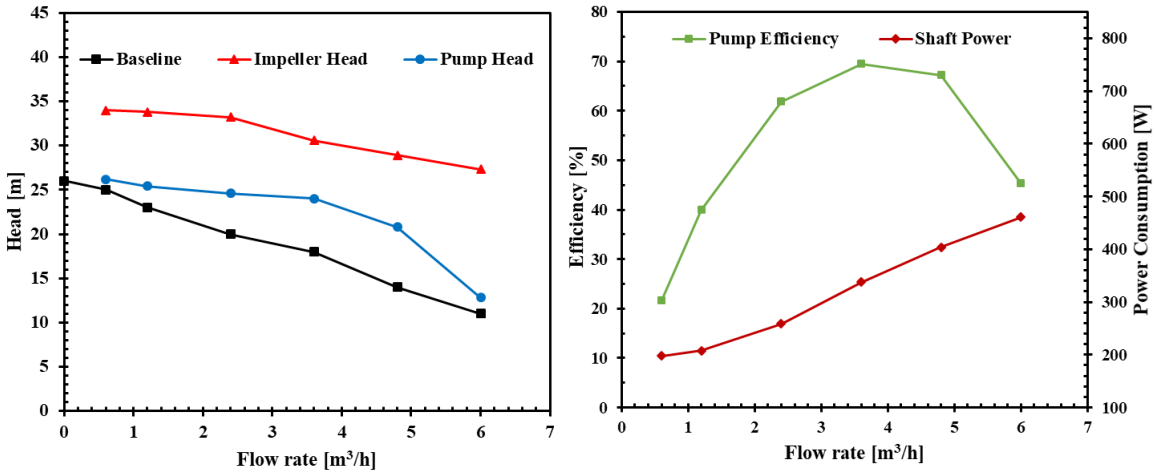

(a) Q-H curves (b) Efficiency and shaft power

Figure 4.2 Performance curves of the centrifugal pump

4.1 Flow Recirculation at Part load Conditions

The performance data shows very low efficiency of the pump operating at part load conditions. This is due to sharp increase in shaft power consumption at this operating condition. Due to impeller- volute interaction, the radial forces at impeller periphery occur that suddenly increases the power absorption at part-load condition. In Fig. 4.3 (a) velocity streamlines shows the flow recirculation from volute to inlet pipe. At higher flow rate, smooth streamlines start from inlet, but the flow vortices appear at volute exit as shown in Fig. 4.3 (b).

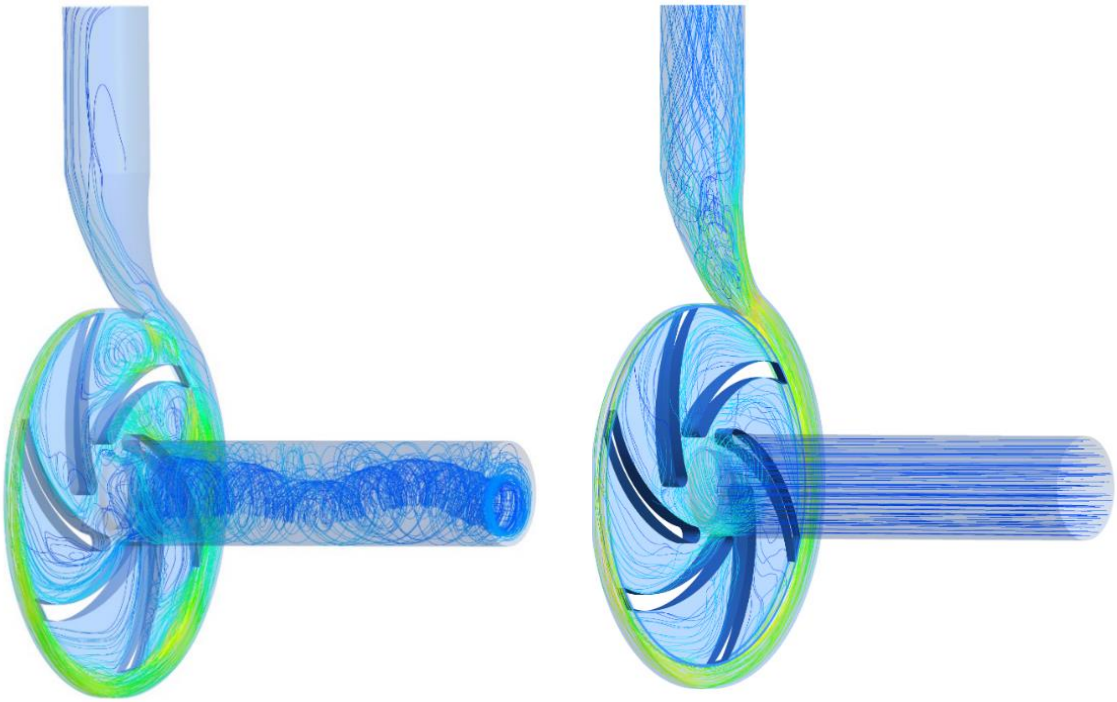

(a) Part load conditions (b) Design condition

Figure 4.3 Velocity streamlines at various operating conditions

4.2 Volute Design Methods

The first step in volute design is to calculate the spiral cross-sectional areas. The two methods commonly used are constant velocity and constant angular momentum methods. First is proposed by Stepanoff and second by Pfleiderer. The first method is mostly preferred for low specific speed and second for high specific speed pumps. In this method, the tangential component of absolute velocity at the impeller outlet is used the spiral design.

The wrap angle of single volute is 360º and the clearance between impeller and cutwater is very small ($\approx 1mm$) in this pump. The volute main dimensions are shown in Fig. 4.4. Due to manufacturing constraints, the volute rectangular cross-sectional shape is not changed. Other shapes may include circular, flat and trapezoidal cross-sections. The outer diameter of the discharge nozzle will not be changed. The geometric dimensions of the volute are given in Table 4.1.

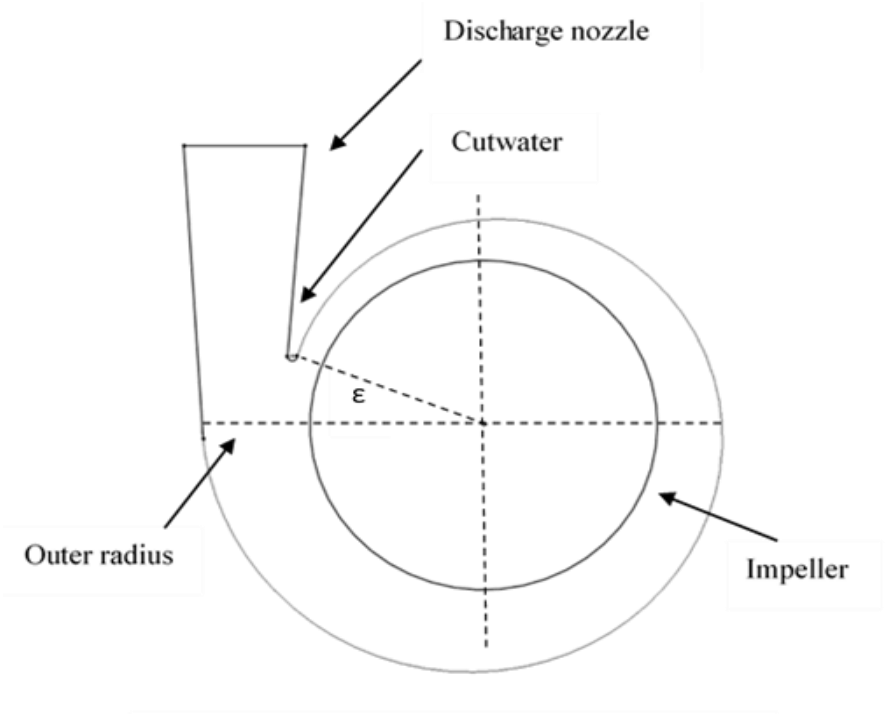

Figure 4.4 Volute main dimensions

Table 4.1. Geometric dimensions of the volute

Description	**Value**
Radial Gap (mm)	1
Inlet width (mm)	5.5
Discharge nozzle height (mm)	121
Outlet diameter (mm)	31
Cutwater position (deg)	11

4.3 Radial Thrust due to Non-uniform Pressure Distribution

The non-uniform pressure generates radial thrust over the impeller circumference. The radial thrust generated at various operating conditions are discussed below:

1. At part load ($Q < Q_{des}$) the volute area is larger for incoming flow from the impeller so the fluid will be decelerated, and static pressure increases in the volute from cutwater to throat area as can be seen in Fig. 4.5 (a). This non-uniform pressure around the impeller periphery generates the maximum radial thrust at low flow rates.

2. At design flow rare ($Q = Q_{des}$), the flow from impeller smoothly enters the volute cutwater. The flow deceleration occurs smoothly, and the pressure distribution is almost uniform. This will result in a very low radial forces around the impeller periphery as can be seen in Fig. 4.6.

3. At higher flow conditions ($Q > Q_{des}$) the volute cross sectional area is smaller for the incoming flow from impeller. The flow will be accelerated downstream of the impeller. The static pressure decreases in circumferential direction from a maximum (stagnation pressure) at the cutwater. The approach flow angle to the cutwater is too large (negative incidence) generating a flow separation in the discharge nozzle.

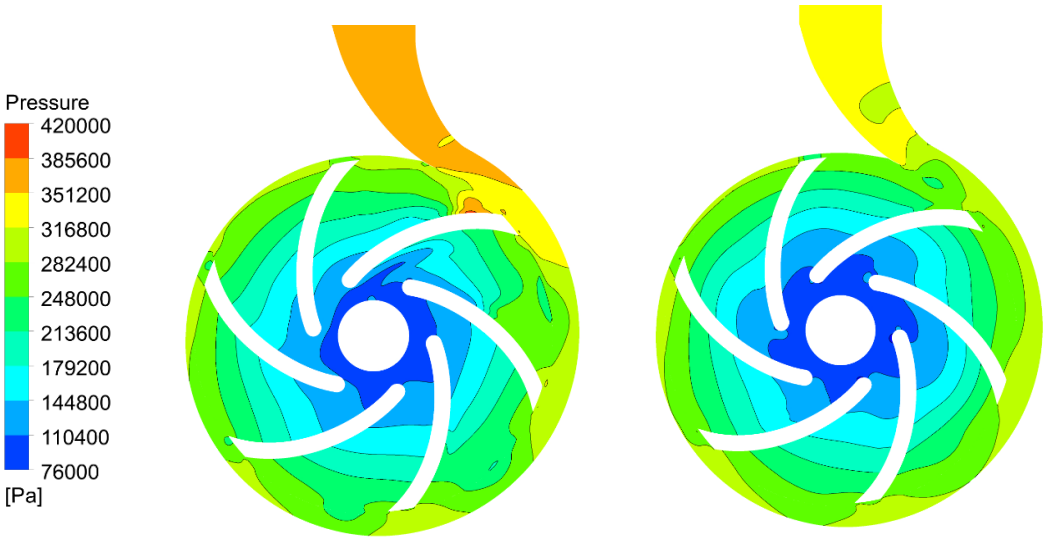

(a) Low flow rate (b) High flow rate

Figure 4.5 Static pressure contours for different operating conditions

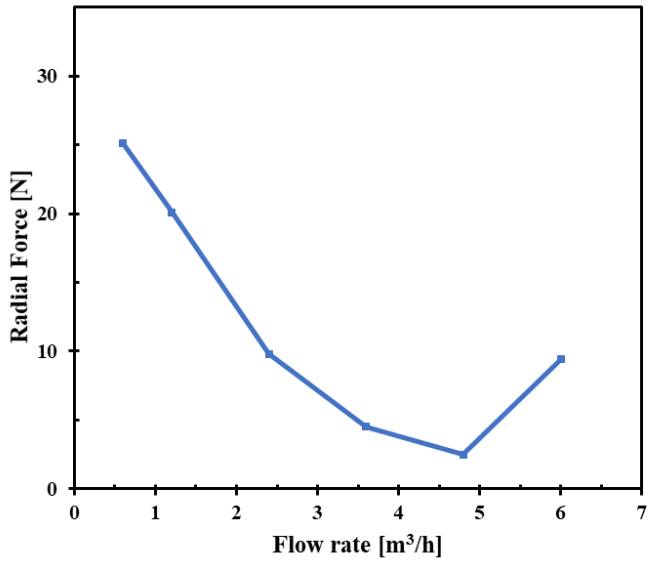

Figure 4.6 Radial force acting on the periphery of the impeller at various flow rates

4.4 Volute with Different Discharge Nozzle

The discharge nozzle/diffuser of the volute may be radial or tangential and each can be chosen depending on the application. Fig. 4.7 shows comparison of performance for pumps with radial and tangential discharge nozzle. The static pressure contours and relative velocity contours for radial and tangential nozzles are shown in Fig. 4.8 and Fig. 4.9 respectively.

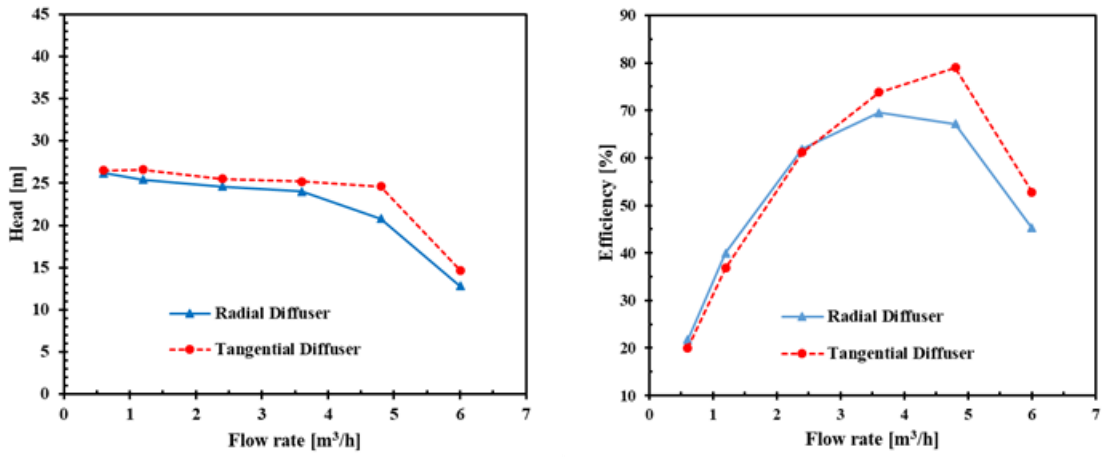

(a) Q-H curves (b) Efficiency and shaft power

Figure 4.7 Comparison of the performance of pump with radial and tangential discharge nozzle

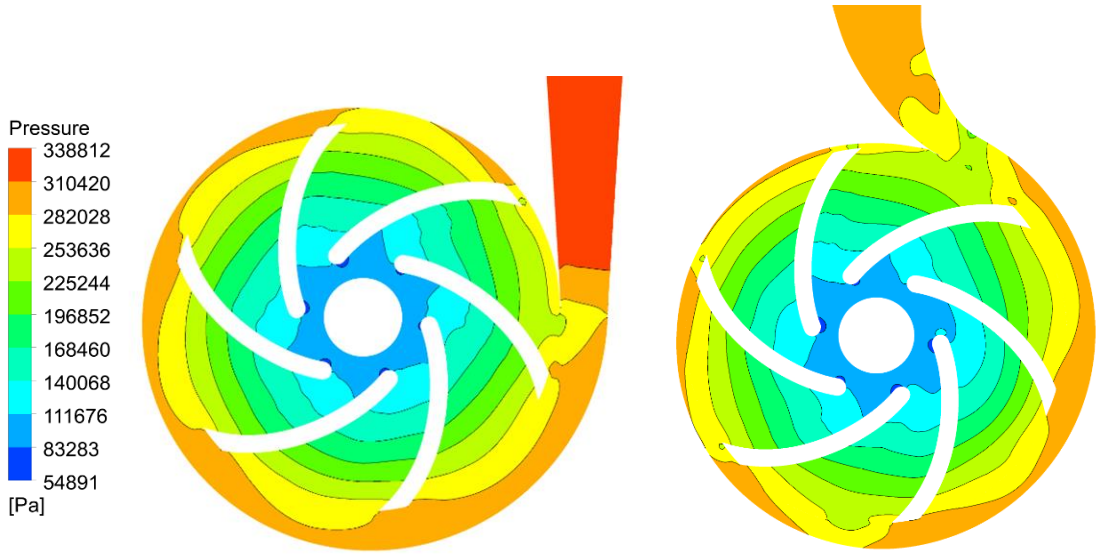

(a) Tangential discharge nozzle (b) Radial discharge nozzle

Figure 4.8 Static pressure contours in pump at design condition with different discharge nozzle

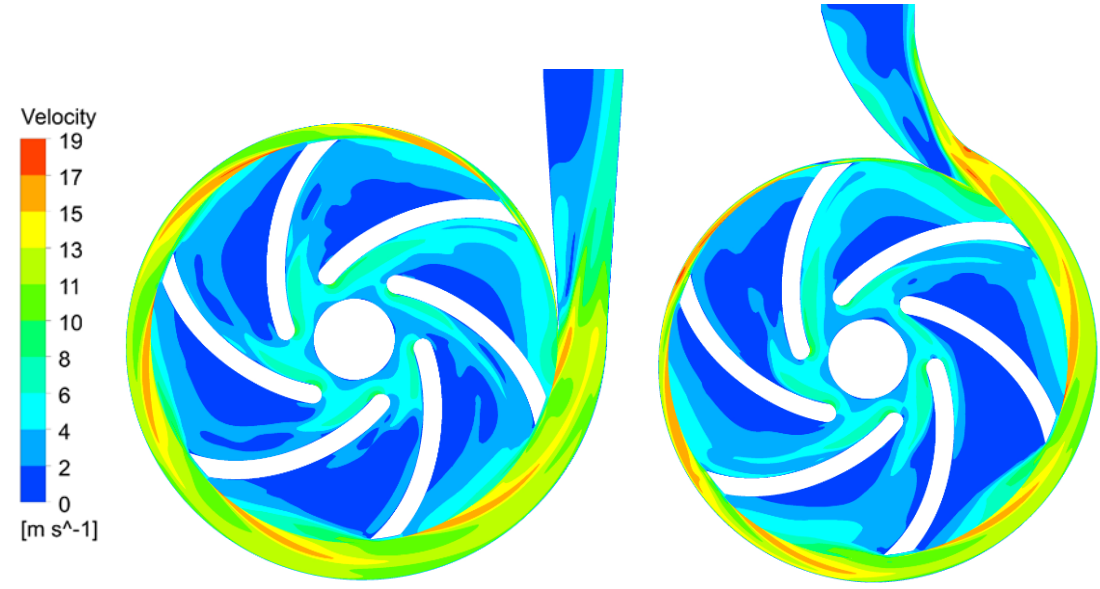

(a) Tangential discharge nozzle (b) Radial discharge nozzle

Figure 4.9 Relative velocity contours in pump at design condition with different discharge

Summary

In this chapter, the hydraulic performance of the full pump model with volute is analyzed. The asymmetric shape of the volute has significant impact on the flow field inside the impeller and volute. The volute is redesigned to reduce the secondary losses. An iterative process in which volute cross-section, spiral shape and discharge nozzle shape is changed step by step to see their effect on the performance of the centrifugal pump. The significant change is observed by changing the discharge nozzle type. The volute with tangential discharge nozzle gains a substantial 8.5% efficiency and 3.2m head improvement as compared to the original pump.

Chapter 5

Cavitation Analysis of Centrifugal Pump

5.1 Cavitation

Cavitation is an important phenomenon to study in centrifugal pumps which disrupts the primary flow due to vapor cavities inside pump. Intense cavitation can lead to material erosion and produces noise and vibrations when the vapor filled ones (bubbles) implodes on the material surface. In terms of improvement in cavitation performance, the inlet blade angle is considered as design parameter as it directly influences the inlet flow conditions.

5.2 Net Positive Suction Head

Net positive suction head (NPSH) is the difference of total head at suction port and the vapor pressure head of the fluid at given temperature.

$$NPSH = \frac{P_{in}}{\rho g} + \frac{{v_{in}}^2}{2g} - \frac{P_v}{\rho g} \tag{5.1}$$

where P_{in} and v_{in} are absolute inlet pressure and inlet velocity respectively; ρ is the density and P_v is vapor pressure (P_v=3574 Pa at 25℃) of the fluid. The $NPSH_3$ is accepted as a criterion of cavitation when the head drops by 3% of the actual head developing without cavitation. The development of cavitation is simulated only at design flow condition. For better cavitation performance, $NPSH_3$ must be small. When the static pressure falls below the saturation pressure of the fluid, vapor cavities start growing at various cross sections of the blades with different size and intensity.

As the cavitation phenomena is linked to static pressure, the first approach is to see the static pressure distribution in the impeller without cavitation. Fig. 5.1 shows the blade loading diagram in which static pressure variation is given along the streamline. At inlet pressure of 1 atm, the pressure is dropped to 58,000 Pa near the throat area of blades. Therefore, when the pump sucks the fluid from 5 m or below the surface of pump, the

pressure at the inlet will already be dropped to about 30,000 Pa as calculated from the Bernoulli's equation. When this low-pressure fluid reached the throat area of the blades, there is greater probability that pressure drops below the saturation pressure of fluid.

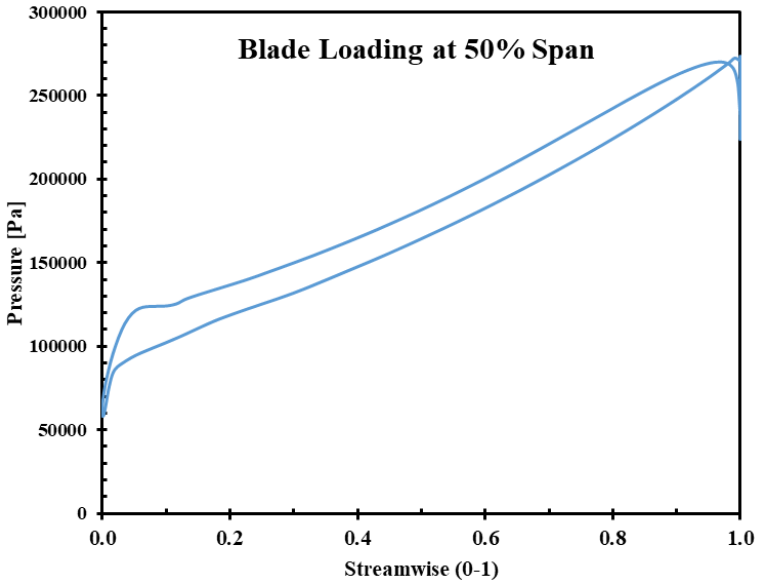

Figure 5.1 Blade loading diagram for non-cavitating conditions

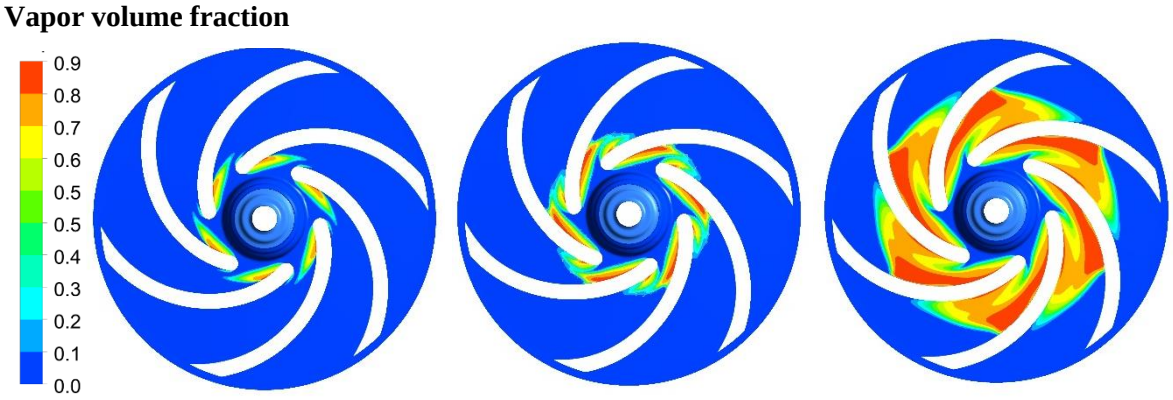

(a) Inlet pressure 12000 Pa (b) Inlet pressure 9000 Pa (c) Inlet pressure 8000 Pa

Figure 5.2 Vapor volume fraction for decreasing inlet

For inlet total pressure equal to 20000, 16000, 12000 Pa, thin vapor cavities start to develop at the suction side of blade near the leading edge. When lowering the total inlet pressure to 9000 Pa, the long and thick cavities develop that disturbs the flow in impeller as shown in Fig. 5.2.

5.3 Effect of Inlet Blade Angle on Cavitation

Initially, the head drop curve at inlet blade angle of 26º is drawn which shows sudden head drop when lowering the inlet pressure reaches a certain level. The $NPSH_3$ of original pump was 2.78 m. For better cavitation performance, NPSH must be low. The inlet angle controls the inflow conditions in the impeller blades at different operating condition, is selected as design variable to improve the cavitation phenomena. The inlet blade angle is decreased from 26º to 18º and it showed positive effect on cavitation resistance. The head drop curves with decreasing inlet blade angle is compared in Fig. 5.3. The $NPSH_3$ 1.66 m for the optimal pump is achieved with inlet blade angle of 18º.

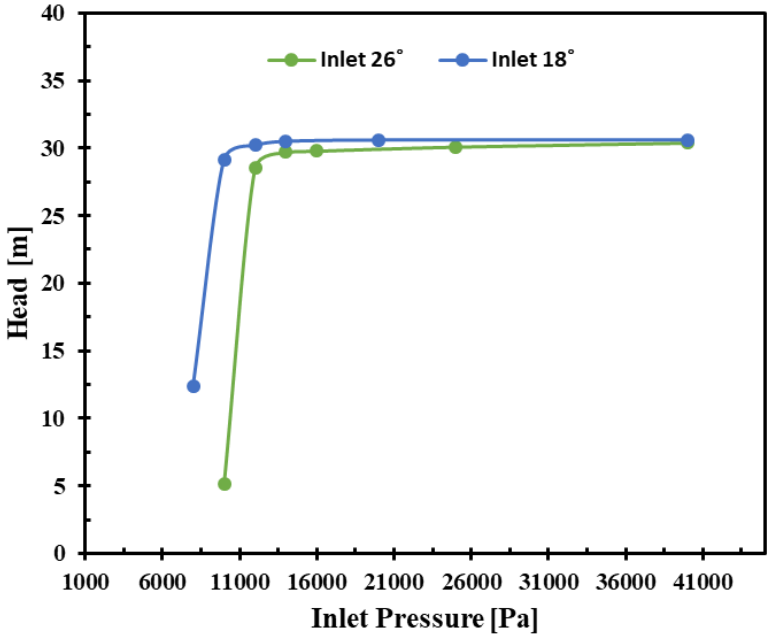

Figure 5.3 Head-drop curves for varying blade inlet angles

Summary

In this chapter, the two-phase flow inside the pump is investigated. The cavitation of the pump is sensitive to inlet flow conditions. Therefore, the blade inlet angle is optimally selected to improve the cavitation performance of the pump. For better cavitation resistance, NPSH of the pump must be low. The NPSH of pump impeller with inlet angle 18º gives 1.12 m decline as compared to the baseline pump.

Chapter 6

Conclusions and Recommendations

6.1 Conclusions

The CFD analysis of low specific speed centrifugal pump has been done to extract the performance of the baseline model pump. This research work analyzes the flow field in centrifugal pump by varying impeller design parameters and volute design shape to improve its hydraulic performance. The sensitivity of pump performance on blade wrap angle and blade outlet angle is observed.

1) The impeller with large blade wrap angle of 110º significantly reduces the flow separation occurring on the pressure side of the blades. Therefore, impeller with wrap angle of 110º consumes the least shaft power. Also due to large flow passage between the blades, the frictional losses are higher as compared to the original pump impeller and head of the pump drops marginally.

2) The blade outlet angle being a sensitive parameter for the pump performance, as described by the Euler equation, is varied from 22º to 50º. With large outlet angle, the swirl component $c_{\theta 2}$ increases which produces higher head of the pump.

3) The improved impeller design with blade wrap angle of 110º and outlet angle of 50º gives an improvement in hydraulic efficiency of 0.6% rise as compared to original impeller.

4) The asymmetric volute shape has a strong effect on the flow field inside the impeller. The rotor-stator interaction produces non-uniform flow field which leads to radial thrust acting on the periphery of the impeller at part load conditions.

5) The performance of pump volute with radial and tangential discharge nozzle is compared. The best efficiency point of pump with tangential discharge nozzle shifts

to high flow rate but gains a significant 8.5% efficiency rise as compared to radial discharge nozzle.

6) The specific characteristics of asymmetric blade cavitating patterns at design flow rate is observed. The cavitation performance is also improved by decreasing inlet blade angle. The inlet blade angle of 18º gives $NPSH_3$ of 1.12 m decline as compared to original pump.

6.2 Recommendations for Future Work

This research work mainly focuses to improve the hydraulic efficiency of centrifugal pump at design condition. The flow analysis at off-design conditions especially stall condition at part load operation is an important aspect to study that greatly impairs the pump performance.

Also, the unsteady flow analysis gives the in-depth investigation of the flow behavior as the impeller position continuously change with respect to cutwater. The pressure pulsations, noise and vibrations are the problems that mostly encountered in the pumps.

In this work, the impeller side casing is not included in the computational domain. If the leakage losses and axial thrust are to analyze, then this must be included in the domain.

Chapter 7

OSU Research Work

7.1 Condensation Phase Change Module

The objective of condensation heat transfer facility is to study two phase flow regimes for different refrigerants and to measure the heat transfer coefficient of different refrigerants. In condensation heat transfer facility, subcooled liquid refrigerant is pumped with a gear pump through a coiled tube and tube evaporator. At evaporator outlet, the sight glass ensures the superheated state of refrigerant. This superheated refrigerant then enters the test section, where it exchanges heat with water. The heat duty of test section can be calculated from the counter flow water loop. In test section refrigerant is partially condensed to study two phase flow and after exiting test section at 2, the two-phase mixture is then fully condensed in the post tube and tube condenser before returning to gear pump. A nitrogen charged piston accumulator was used to maintain the desired saturated pressure.

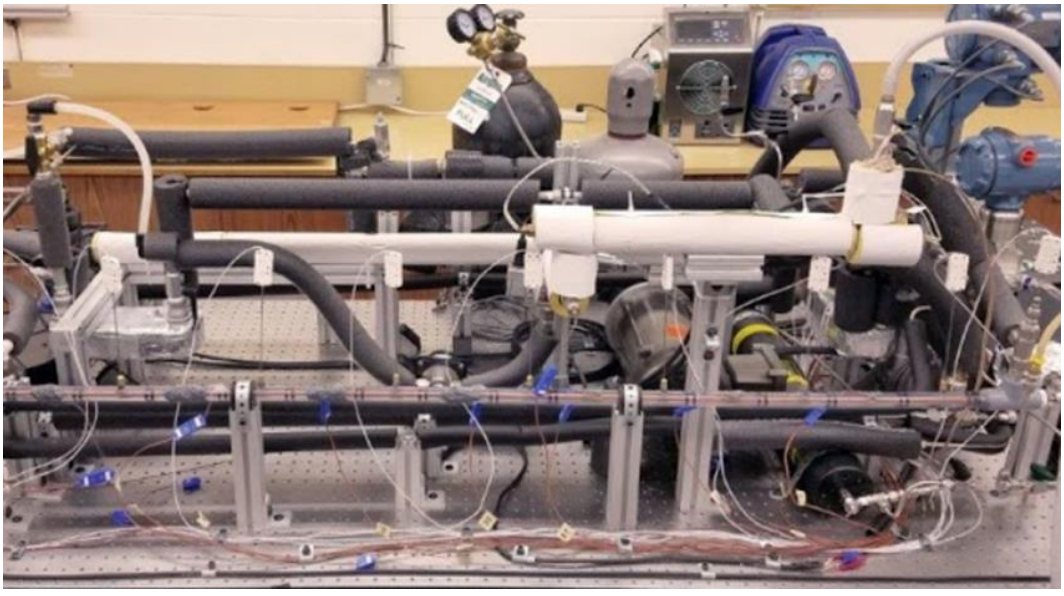

Figure 7.1 Experimental setup for condensation test facility

7.2 Supercritical Heat Transfer Facility

The objective of this facility is to experimentally determine the heat transfer coefficient using supercritical carbon dioxide fluid in microchannels with non-uniform heat flux. In supercritical carbon dioxide heat transfer facility, the fluid is pumped through a gear pump through a Coriolis flow meter to measure the flow rate and it then enters the preheaters where heat is provided to control inlet fluid temperature to test section. In test section non-uniform heat flux is provided by cartridge heater and this flux is calculated using thermocouples. Using resistance network and COMSOL simulations we can find heat transfer coefficient. The hot vapor like fluid is then cooled in tube in tube post cooler and then cycle is maintained by recirculating the fluid through loop by pumping it through gear pump. A nitrogen charged piston accumulator was used to maintain the system pressure. The data is then collected in LABVIEW software using DAQ card for data acquisition.

Figure 7.2 Experimental setup for supercritical heat transfer

7.3 Fluke Calibrator

In fluke calibrator, thermocouples are calibrated by comparing the data with the standard thermocouple probe. First of all, standard thermocouple probe is dip in the silicon bath of calibrator. Then the thermocouples to be calibrated, are dipped in that bath and data is collected in the LABVIEW.

Figure 7.3 Test probe and fluke calibrator

References

[1] J. F. Gulich, "Centrifugal Pumps," (3rd Edition), *Springer*, pp. 79–497, 2014.

[2] Y. Xu, L. Tan, S. Cao, and W. Qu, "Multiparameter and multiobjective optimization design of centrifugal pump based on orthogonal method," *Proc. Inst. Mech. Eng. Part C J. Mech. Eng. Sci.*, vol. 231, no. 14, pp. 2569–2579, 2017.

[3] Y. Fu *et al.*, "Numerical and experimental analysis of flow phenomena in a centrifugal pump operating under low flow rates," *J. Fluids Eng. Trans. ASME*, vol. 137, no. 1, 2015.

[4] A. H. Dönmez, Z. Yumurtaci, and L. Kavurmacioglu, "The effect of inlet blade angle variation on cavitation performance of a centrifugal pump: A parametric study," *J. Fluids Eng. Trans. ASME*, vol. 141, no. 2, 2018.

[5] L. Tan, B. Zhu, S. Cao, H. Bing, and Y. Wang, "Influence of blade wrap angle on centrifugal pump performance by numerical and experimental study," *Chinese J. Mech. Eng. (English Ed.*, vol. 27, no. 1, pp. 171–177, 2014.

[6] E. C. Bacharoudis, A. E. Filios, M. D. Mentzos, and D. P. Margaris, "Parametric Study of a Centrifugal Pump Impeller by Varying the Outlet Blade Angle," *Open Mech. Eng. J.*, vol. 2, no. 1, pp. 75–83, 2008.

[7] J. Pei, W. Wang, S. Yuan, and J. Zhang, "Optimization on the impeller of a low-specific-speed centrifugal pump for hydraulic performance improvement," *Chinese J. Mech. Eng. (English Ed.*, vol. 29, no. 5, pp. 992–1002, 2016.

[8] H. S. Shim, K. Y. Kim, and Y. S. Choi, "Three-Objective Optimization of a Centrifugal Pump to Reduce Flow Recirculation and Cavitation," *J. Fluids Eng. Trans. ASME*, vol. 140, no. 9, 2018.

[9] K. W. Cheah, T. S. Lee, S. H. Winoto, and Z. M. Zhao, "Numerical Analysis of Impeller-Volute Tongue Interaction and Unsteady Fluid Flow in a Centrifugal Pump," *Fluid Mach. Fluid Mech.*, no. 4, pp. 66–71, 2009.

[10] J. D. H. Kelder, R. J. H. Dijkers, B. P. M. Van Esch, and N. P. Kruyt, “Experimental and theoretical study of the flow in the volute of a low specific-speed pump,” *Fluid Dyn. Res.*, vol. 28, no. 4, pp. 267–280, 2001.

[11] H. Alemi, S. A. Nourbakhsh, M. Raisee, and A. F. Najafi, “Development of new ‘multivolute casing’ geometries for radial force reduction in centrifugal pumps,” *Eng. Appl. Comput. Fluid Mech.*, vol. 9, no. 1, pp. 1–11, 2015.

[12] W. Cao, L. Yao, B. Liu, and Y. Zhang, “The influence of impeller eccentricity on centrifugal pump,” *Adv. Mech. Eng.*, vol. 9, no. 9, pp. 1–17, 2017.

[13] FeiZhao, F. Kong, Yisong Zhou, Bin Xia, and Yuxing Bai, “Optimization Design of the Impeller in Ultra_Low Specific Speed Magnetic Drive Pump,” 2019.

[14] J. F. Combes, A. Boyer, L. Gros, D. Pierrat, G. Pintrand, and P. Chantrel, “Experimental and Numerical Investigations of the Radial Thrust in a Centrifugal Pump,” pp. 1–7, 2008.

[15] M. Zangeneh, A. Goto, and H. Harada, “On the design criteria for suppression of secondary flows in centrifugal and mixed flow impellers,” *Proc. ASME Turbo Expo*, vol. 1, no. October 1998, pp. 723–735, 1997.

[16] R. K. Byskov, C. B. Jacobsen, and N. Pedersen, “Flow in a centrifugal pump impeller at design and off-design conditions - Part II: Large eddy simulations,” *J. Fluids Eng. Trans. ASME*, vol. 125, no. 1, pp. 73–83, 2003.

[17] W. Ye, X. Luo, R. Huang, Z. Jiang, X. Li, and Z. Zhu, “Investigation of flow instability characteristics in a low specific speed centrifugal pump using a modified partially averaged Navier–Stokes model,” *Proc. Inst. Mech. Eng. Part A J. Power Energy*, vol. 233, no. 7, pp. 834–848, 2019.

[18] Z. An, L. Zhounian, W. Peng, C. Linlin, and W. Dazhuan, “Multi-objective optimization of a low specific speed centrifugal pump using an evolutionary algorithm,” *Eng. Optim.*, vol. 48, no. 7, pp. 1251–1274, 2016.

[19] C. Lettieri, J. Defoe, and Z. S. Spakovszky, “An investigation of nonlinear flow

oscillations in a high-pressure centrifugal pump," *J. Turbomach.*, no. 11, 2015.

[20] M. Benturki, R. Dizene, and A. Ghenaiet, "Multi-objective optimization of two-stage centrifugal pump using NSGA-II algorithm," *J. Appl. Fluid Mech.*, vol. 11, no. 4, pp. 929–943, 2018.

[21] J. Friedrichs and G. Kosyna, "Rotating cavitation in a centrifugal pump impeller of low specific speed," *J. Fluids Eng. Trans. ASME*, vol. 124, no. 2, pp. 356–362, 2002.

[22] Y. Li, X. Li, Z. Zhu, and F. Li, "Investigation of unsteady flow in a centrifugal pump at low flow rate," *Adv. Mech. Eng.*, vol. 8, no. 12, pp. 1–8, 2016.

[23] F. Magagnato and J. Zhang, "Simulation of a centrifugal pump by using the harmonic balance method," *Int. J. Rotating Mach.*, vol. 2015, no. May, 2015.

[24] S. Yang, F. Kong, and B. Chen, "Research on pump volute design method using CFD," *Int. J. Rotating Mach.*, vol. 2011, 2011.

[25] H. Alemi, S. A. Nourbakhsh, M. Raisee, and A. F. Najafi, "Effects of volute curvature on performance of a low specific-speed centrifugal pump at design and off-design conditions," *J. Turbomach.*, vol. 137, no. 4, 2015.

[26] S. A. Nourbakhsh and R. Torabi, "Hydrodynamic Design of the Volute of a Centrifugal PUMP Using CFD," vol. 60, pp. 1–5, 2011.

[27] R. Spence and J. Amaral-Teixeira, "Investigation into pressure pulsations in a centrifugal pump using numerical methods supported by industrial tests," *Comput. Fluids*, vol. 37, no. 6, pp. 690–704, 2008.

[28] X. Han, Y. Kang, D. Li, and W. Zhao, "Impeller optimized design of the centrifugal pump: A numerical and experimental investigation," *Energies*, vol. 11, no. 6, 2018.

[29] C. E. Brennen, "Hydrodynamics of Pumps," (9th Edition), *Cambridge*, pp. 133-217, 2011.

[30] E. M. Greitzer, "The Stability of Pumping Systems," *J. Fluids Eng.*, vol. 103, no.

June, p. 193, 1981.

[31] F. J. Wiesner, “A review of slip factors for centrifugal impellers,” *J. Eng. Gas Turbines Power*, vol. 89, no. 4, pp. 558–566, 1967.

[32] Breugelmans F.A and M. Sen, “Prerotation and Fluid Recirculation in the Suction Pipe of Contrifugal Pumps,” pp. 165–180, 1977.

[33] D. Cowan and S. Bradshaw, “Influence of Impeller Suction Specific Speed on Vibration Performance,” pp. 1–15, 2013.

[34] B. Schiavello and Frank C.Visser, “PUMP CAVITATION—VARIOUS NPSHR CRITERIA, NPSHA MARGINS, AND IMPELLER LIFE EXPECTANCY.pdf.” pp. 114–144, 25th International Pump Users Symposium, 2009.

[35] R. Hirschi *et al.*, “Centrifugal pump performance drop due to leading edge cavitation: Numerical predictions compared with model tests,” *Am. Soc. Mech. Eng. Fluids Eng. Div. FED*, vol. 11, no. December 1998, 1997.

[36] R. Franz, A. J. Acosta, C. E. Brennen, and T. K. Caughey, “The rotordynamic forces on a centrifugal pump impeller in the presence of cavitation,” *J. Fluids Eng. Trans. ASME*, vol. 112, no. 3, pp. 264–271, 1990.

[37] D. Bonaiuti and M. Zangeneh, “On the coupling of inverse design and optimization techniques for the multiobjective, multipoint design of turbomachinery blades,” *J. Turbomach.*, vol. 131, no. 2, pp. 1–16, 2009.

[38] J. A. Lorett and S. Gopalakrishnan, “Interaction between impeller and volute of pumps at off-design conditions,” *J. Fluids Eng. Trans. ASME*, vol. 108, no. 1, pp. 12–18, 1986.

[39] T. D. Canonsburg, “ANSYS CFX Reference Guide,” vol. 15317, no. April, pp. 724–746, 2009.

[40] ANSYS Inc., “Turbulence Modeling in Fluent,” 15.0 Release, pp. 1–48, 2014.

Appendices

A. Mathematical Calculations

```
"Golden Pump GMB-71-1/0.37"
g=9.81 [m/s^2]
T_in=25 [C]
p_in=101.325 [kPa]
rho=density(WATER,T=T_in,p=p_in)
mu=viscosity(WATER,T=T_in,p=p_in)
p_v=p_sat(WATER,T=T_in)*convert(kPa,Pa)
P_elec=0.37[kW]
d_i=1.25[in]*convert(in,m)  "Internal Pipe dia"
epsilon=0.0046 [cm]*convert(cm,m)    "Absolute roughness of commercial steel"

"Suction lift"          "Head"          "Volume flow rate"
z_s[1]=8 [m];           H[1]=26 [m];    V_dot[1]=0 [m^3/h]
z_s[2]=7.5 [m];         H[2]=25 [m];    V_dot[2]=0.6 [m^3/h]
z_s[3]=7 [m];           H[3]=23 [m];    V_dot[3]=1.2 [m^3/h]
z_s[4]=6.5 [m];         H[4]=20 [m];    V_dot[4]=2.4 [m^3/h]
z_s[5]=6 [m];           H[5]=18 [m];    V_dot[5]=3.6 [m^3/h]
z_s[6]=5.5 [m];         H[6]=14 [m];    V_dot[6]=4.8 [m^3/h]
z_s[7]=5 [m];           H[7]=11 [m];    V_dot[7]=6 [m^3/h]


"Assuming motor efficiency of 65% with 2900RPM"
eta_motor=0.65
P_bhp=(P_elec*eta_motor)*convert(kW,W)

Duplicate i=1,7

 P_hyd[i]=rho*g*H[i]*V_dot[i]*convert(m^3/h,m^3/s)
 eta_pump[i]=(P_hyd[i]/P_bhp)*100

 V_dot[i]*convert(m^3/h,m^3/s)=pi*d_i^2*v_s[i]/4

 "Determination of friction factor from Moody Diagram"
 Re[i]=rho*v_s[i]*d_i/mu

 f[i]=Moodychart(Re[i],epsilon/d_i)

 "Friction losses in suction piping"
 h_f[i]=f[i]*z_s[i]*v_s[i]^2/(2*g*d_i)

 "Applying Bernoulli equation at suction port of the pump"
 p_in*convert(kpa,pa)/(rho*g)=p_s[i]/(rho*g)+v_s[i]^2/(2*g)+z_s[i]+h_f[i]

 "Total pressure at inlet"
 p_tot[i]=p_s[i]+(rho/2)*(v_s[i])^2

 "NPSH calculation"
 NPSHA[i]=(p_tot[i]-p_v)/(rho*g)

End
```

SOLUTION

Unit Settings: SI C kPa kJ mass deg

d_i = 0.03175 [m]	ε = 0.000046 [m]	η_{motor} = 0.65
g = 9.81 [m/s^2]	μ = 0.0008905 [kg/m-s]	P_{bhp} = 240.5 [W]
P_{elec} = 0.37 [kW]	p_{in} = 101.3 [kPa]	p_v = 3169 [Pa]
ρ = 997.1 [kg/m^3]	T_{in} = 25 [C]	

No unit problems were detected.

EES suggested units (shown in purple) for p_tot[1] p_tot[2] p_tot[3] p_tot[4] p_tot[5] p_tot[6] .

Arrays Table: Main

	$\eta_{pump,i}$	f_i	H_i [m]	$h_{f,i}$ [m]	$NPSHA_i$ [m]	$P_{hyd,i}$ [W]	$p_{s,i}$ [Pa]	$p_{tot,i}$ [Pa]	Re_i	$\dot{V}_i$ [m³/h]
1	0	1.197E+33	26	3.479E-38	2.035	0	23076	23076	5.349E-32	0
2	16.95	0.03576	25	0.01908	2.516	40.75	27757	27780	7483	0.6
3	31.18	0.03068	23	0.0611	2.974	74.99	32171	32259	14967	1.2
4	54.23	0.0272	20	0.2013	3.334	130.4	35425	35779	29934	2.4
5	73.21	0.02574	18	0.3956	3.64	176.1	37973	38769	44900	3.6
6	75.92	0.02492	14	0.6239	3.911	182.6	40012	41426	59867	4.8
7	74.56	0.02437	11	0.867	4.168	179.3	41730	43939	74834	6

Arrays Table: Main

	$v_{s,i}$ [m/s]	$z_{s,i}$ [m]
1	1.505E-36	8
2	0.2105	7.5
3	0.421	7
4	0.842	6.5
5	1.263	6
6	1.684	5.5
7	2.105	5

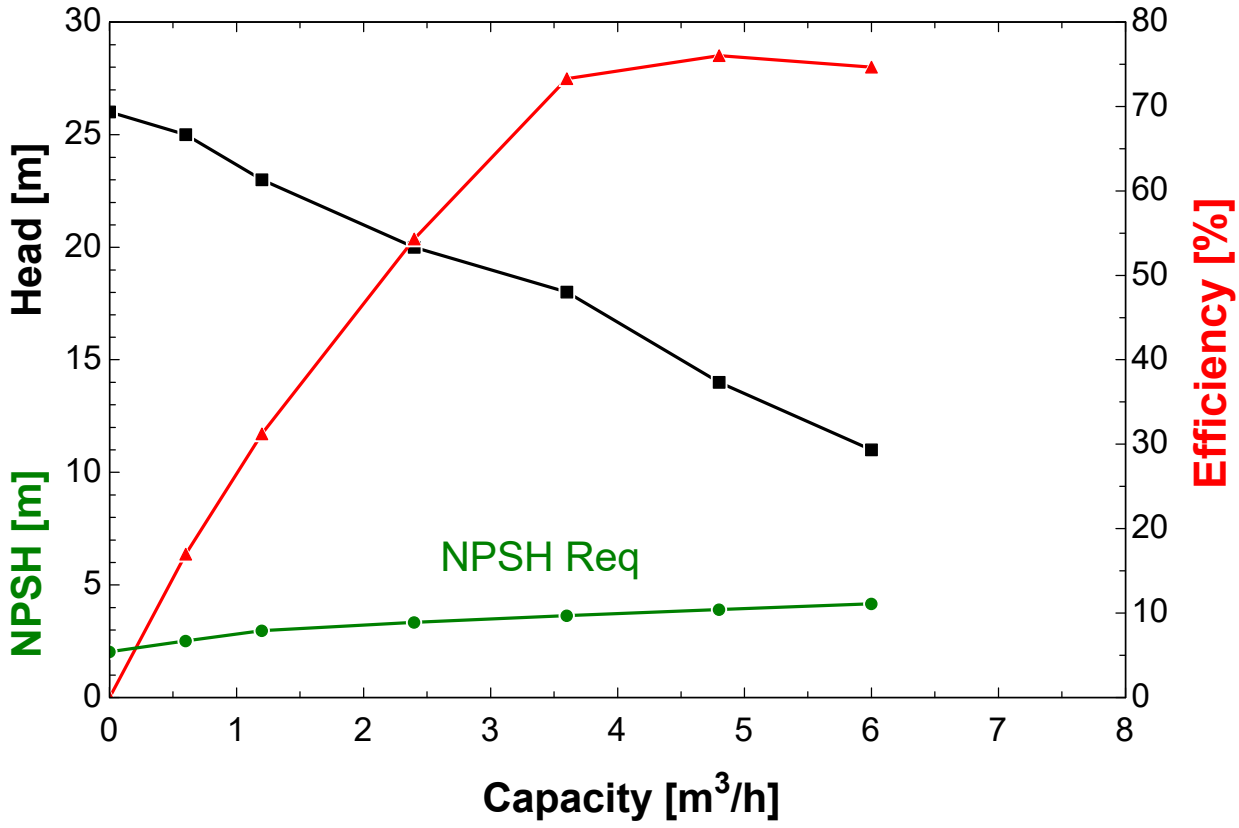

B. Impeller Design Code

```
Function factor(d_1m_dot,epsilon_lim)
 If d_1m_dot<epsilon_lim Then
 factor=1
 Else
 factor=1-((d_1m_dot-epsilon_lim)/(1-epsilon_lim))^3
 Endif
End

"!Design Conditions"
N=1450 "[RPM]"
Q_opt=200 [m^3/h]*convert(m^3/h,m^3/s)
H_opt=20 [m]
g=9.81 [m/s^2]
rho=density(Water,T=20[C],P=101.325[kPa])
mu=viscosity(Water,T=20[C],P=101.325[kPa])
alpha_1=90 [degree]

"!Table 7.1: Impeller Calculation"
"Specific Speed"
f_q=1  "single entry impeller"
j=1 [m^0.75]                    "!For unit conversion"
o=1 [s^0.5]                     "!For unit conversion"
N_q=(N*sqrt(Q_opt/f_q)/(H_opt)^0.75)*o/j


"Assumed Hydraulic efficiency"
Q_ref=1 [m^3/s]
a=1
m=0.08*a*((Q_ref/Q_opt)^0.15)*((45/N_q)^0.06)
eta_hyd=1-0.055*((Q_ref/Q_opt)^m)-0.2*(0.26-log10(N_q/25))^2*(Q_ref/Q_opt)^0.1

"Impeller flow rate"
a_sp=0.15
m_sp=0.6
z_h=1                                   "Without balance holes"
Q_sp=Q_opt*a_sp*z_h/N_q^m_sp      "leakage flow rate through seal at impeller inlet"
Q_e=0                                   "flow rate through axial thrust balancing device"
Q_la=Q_opt+Q_sp+Q_e

"Volumetric efficiency"
eta_vol=Q_opt/Q_la

"Shaft Dia"
tau_shear=450 [MPa]*convert(MPa,Pa)       "Shear Strength of Stainless Steel (X20Cr13) 1.4021"
FOS=1.8
tau_al=tau_shear/FOS

P_max=rho*g*H_opt*Q_opt/eta_hyd
p=1 [1/s]                                 "!For unit conversion"
omega=2*pi*N*p/60
d_w=((16*P_max)/(pi*omega*tau_al))^(1/3)

"Head Coefficient"
f_t=1.1
N_q_ref=100
Si_opt=1.21*f_t*exp(-0.77*N_q/N_q_ref)

"Impeller Outlet Dia"
d_2=(2/omega)*sqrt(2*g*H_opt/Si_opt)

"Number of blades"
z_la=5
```

```
"Blade thickness"
e_1=0.018*d_2    "Leading edge"
e_2=e_1/2        "Trailing edge"

"Impeller Inlet Dia for minimum relative velocity"
f_d1=1.14
lambda_r=1                  "Swirl number"
d_n=d_w+0.005[m]            "Hub Dia"
d_n_dot=d_n/d_2
d_1_dot=f_d1*sqrt(d_n_dot^2+1.48e-3*Si_opt*N_q^1.33/(eta_vol*lambda_r)^0.67)
d_1_dot=d_1o/d_2

"Impeller inlet dia for inner streamline"
d_1i=d_n+0.006[m]

"!Table 3.1: Velocity triangle at Impeller inlet"
d_1b=(d_1o+d_1i)/2                                  "Arithematic average of diameters"
d_1m=sqrt((d_1o^2+d_1i^2)/2)                        "Geometric average of diameters"
A_1=pi*(d_1o^2-d_1i^2)/4
A_1=pi*d_1b*b_1

c_1m=Q_la/(f_q*A_1)                                 "Meridional component of absolute velocity"
c_1u=c_1m/tan(alpha_1)                              "Circumferential component of absolute velocity"

"Outer Streamline"
v=1 [1/s]                                           "!For unit conversion"
u_1o=pi*d_1o*N*v/60                                 "Circumferential Speed"
w_1o=sqrt(c_1m^2+(u_1o-c_1u)^2)                     "Relative velocity"
phi_1=c_1m/u_1o                                     "Flow coefficient"
beta_1o=arctan(c_1m/(u_1o-c_1u))                    "Flow angle without blockage"
i_1=4 [degree]                                      "Incidence"
beta_1b_o=beta_1o+i_1                               "Blade Angle"
lambda_1o=85[degree]                                "Effect of inclination (twisted blades)"
tau_1_o=(1-(z_la*e_1)/(pi*d_1o*sin(beta_1b_o)*sin(lambda_1o)))^(-1)    "Blade blockage at inlet"
beta_1_dot_o=arctan(c_1m*tau_1_o/(u_1o-c_1u))       "Flow angle with blockage"

i_1_dot=beta_1b_o-beta_1_dot_o

"Mean Streamline"
u_1m=pi*d_1m*N*v/60
w_1m=sqrt(c_1m^2+(u_1m-c_1u)^2)
beta_1m=arctan(c_1m/(u_1m-c_1u))
beta_1b_m=beta_1_dot_m+i_1
lambda_1m=87[degree]
tau_1_m=(1-(z_la*e_1)/(pi*d_1m*sin(beta_1b_m)*sin(lambda_1m)))^(-1)
beta_1_dot_m=arctan(c_1m*tau_1_m/(u_1m-c_1u))

"Inner Streamline"
u_1i=pi*d_1i*N*v/60
w_1i=sqrt(c_1m^2+(u_1i-c_1u)^2)
beta_1i=arctan(c_1m/(u_1i-c_1u))
beta_1b_i=beta_1_dot_i+i_1
lambda_1i=90[degree]                                "No twist at inner streamline"
tau_1_i=(1-(z_la*e_1)/(pi*d_1i*sin(beta_1b_i)*sin(lambda_1i)))^(-1)
beta_1_dot_i=arctan(c_1m*tau_1_i/(u_1i-c_1u))


"Outlet blade width"
b_2_dot=0.017+0.262*(N_q/N_q_ref)-0.08*(N_q/N_q_ref)^2+0.0093*(N_q/N_q_ref)^3
b_2_dot=b_2/d_2

"!Table 3.2: Outlet velocity triangle"
u_2=pi*d_2*N*v/60
```

```
A_2=pi*d_2*b_2
c_2m=Q_la/(f_q*A_2)
phi_2=c_2m/u_2
lambda_2=90[degree]
tau_2=(1-(z_la*e_2)/(pi*d_2*sin(beta_2b)*sin(lambda_2)))^(-1)          "Blade blockage at outlet"


"Outlet Angle Beta is calculated on basis of slip factor"
epsilon_lim=exp(-8.16*sin(beta_2b)/z_la)
f_1=0.98
d_1m_dot=d_1m/d_2
k_w=factor(d_1m_dot,epsilon_lim)
gamma=f_1*k_w*(1-sqrt(sin(beta_2b))/z_la^0.7)          "Slip factor"
H_opt=eta_hyd*u_2^2/g*(gamma-(Q_la/(f_q*A_2*u_2*tan(beta_2b)))*(tau_2+(A_2*d_1m_dot*tan(beta_2b)/(A_1*tan(alpha_1)
))))

c_2u=u_2*(gamma-(c_2m*tau_2/(u_2*tan(beta_2b))))
c_2=sqrt(c_2m^2+c_2u^2)
w_2u=u_2-c_2u
w_2=sqrt(c_2m^2+w_2u^2)
alpha_2=arctan(c_2m/c_2u)                    "Absolute outlet angle without blockage"
beta_2_dot=arctan(c_2m*tau_2/w_2u)           "Relative outlet angle with blockage"
beta_2=arctan(c_2m/w_2u)                     "Relative outlet angle without blockage"
lambda_dot=beta_2b-beta_2_dot
lambda=beta_2b-beta_2                        "Deviation angle"

"Blade Loading"
w_1_dot=w_1o/u_2
w_2_dot=w_2/u_2
Xi_eff=2*pi*Si_opt/(eta_hyd*z_la*L_dot*(w_1_dot+w_2_dot))
Xi_al=(40/N_q)^0.77
Xi_eff=0.12*Xi_al
L_dot=L_sch/d_2

"Throat Area"
w_1q=0.8*w_1m
A_1q=Q_la/(f_q*z_la*w_1q)
A_1q=a_1t*b_1


"Blade distance at outlet"
t_2=pi*d_2/z_la          "pitch"
sin(beta_a2)=0.8*sin(beta_2b)
sin(beta_a2)=a_2o/t_2


"!Table 3.6: Frictional Losses of rotating disk"
R=d_2/2
Re=rho*u_2*R/mu
d_sp=0.48*d_2
r_sp=d_sp/2
epsilon=0.15 [cm]*convert(cm,m)          "Roughness of Galvanized Cast iron"
a_f=1
s_ax=0.02*d_2                            "Sidewall gap"
phi_sp=Q_sp/(pi*R^2*u_2)                 "Flow coefficient in impeller sidewall gap"
f_R=(log10(12.5/Re)/log10((0.2*epsilon/R)+(12.5/Re)))^2.15          "Influence of roughness of rotating disk"
f_L=exp(-350*phi_sp*((R/r_sp)^a_f-1))    "Influence of leakage"
t_ax=s_ax
r_w=R
R_n=d_n/2
k_o=1/(1+(r_w/R)^2*sqrt(((r_w+5*t_ax)/R)))
k_RR=(pi*R/(2*Re*s_ax))+(0.0625*(1-k_o)^1.75*f_R*f_L/Re^0.2)          "Disk friction coefficient"
lamda=15[degree]
```

```
P_RR=k_RR*rho*omega^3*R^5/cos(lamda)*(1-(R_n/R)^5)          "Friction power per side of rotating disk"

"!Table 3.8(1): Hydraulic losses in Impeller"
w_av=(2*Q_la)/(f_q*z_la*(a_2o*b_2+A_1q))                    "Average relative velocity in impeller channel"
Re_imp=rho*w_av*L_sch/mu
c_f=0.136/(-log10(0.2*epsilon/L_sch+12.5/Re_imp))^2.15      "Friction coefficient"
D_h=2*(a_2o*b_2+A_1q)/(a_1t+b_1+a_2o+b_2)                   "Hydraulic diameter"
c_d=(c_f+0.0015)*(1.1+4*b_2/d_2)                            "Dissipation coefficient"
2*g*Z_la_R/u_2^2=4*c_d*L_sch/D_h*(w_av/u_2)^2               "Friction and mixing losses"
2*g*Z_la_C/u_2^2=0.3*((w_1m-w_1q)/u_2)^2                    "Shock loss at impeller inlet"
Z_imp=Z_la_R+Z_la_C                                         "Impeller loss"

"!Table 3.7(1): Leakage Losses through annular seal"
d_ref=100[mm]*convert(mm,m)
2*s/d_sp=0.004*(d_ref/d_sp)^0.53                            "Radial Seal clearance"
L_sp=0.13*d_sp                                              "Seal length"

H_p=(u_2^2-u_1o^2+w_1o^2-w_2^2)/(2*g)-Z_imp                 "Static pressure rise in impeller"
y_sp=Re^0.3*s*d_sp/d_2^2*sqrt(s/L_sp)
k_rot_i=0.9*y_sp^0.087                                      "Rotation factor for radially inward flow"
delta_H_sp=H_p-k_rot_i^2*u_2^2/(2*g)*(1-d_sp^2/d_2^2)       "Pressure difference across seal"

zeta_ea=1.1                                                 "Inlet+Outlet loss"
zeta_k=1.1                                                  "Loss per chamber"

"Combine Reynolds Numbers due to circumferential and axial velocity in sidewall gap"
u_sp=pi*d_sp*N*v/60
Re_u=2*s*u_sp*rho/mu
Re_a=2*s*c_ax*rho/mu
Re_c=sqrt(Re_a^2+Re_u^2/4)

f=0.03                                                      "!Fig.3.14 Friction coefficient of Plain seal"
e=1[m]                                                      "!For unit conversion"
c_ax=sqrt((2*g*delta_H_sp)/(zeta_ea+f*L_sp/(2*s)+zeta_k*(d_sp/e)^2*(s/e)^2))   "Axial velocity in sidewall gap"

Q_sp_i=pi*d_sp*s*c_ax

eta_h=H_opt/(H_opt+Z_imp)                                   "Efficiency after including all flow losses"


Function factor (d_1m,dot, ε_lim)

  If ( d_1m,dot < ε_lim ) Then

     factor := 1

   Else

     factor := 1 - [ (d_1m,dot - ε_lim) / (1 - ε_lim) ]^3

  EndIf

End factor
```

Design Conditions

N = 1450 *[RPM]*

$$Q_{opt} = 200 \ [m^3/h] \cdot \left| 0.000277778 \cdot \frac{m^3/s}{m^3/h} \right|$$

$$H_{opt} = 20 \ [m]$$

$$g = 9.81 \ [m/s^2]$$

$$\rho = \rho(\text{water}, T = 20 \ [C], P = 101.325 \ [kPa])$$

$$\mu = \textbf{Visc}(\text{water}, T = 20 \ [C], P = 101.325 \ [kPa])$$

$$\alpha_1 = 90 \ [Degree]$$

Table 7.1: Impeller Calculation

Specific Speed

$f_q = 1$ *single entry impeller*

$j = 1 \ [m^{0.75}]$ **For unit conversion**

$o = 1 \ [s^{0.5}]$ **For unit conversion**

$$N_q = N \cdot \frac{\sqrt{\frac{Q_{opt}}{f_q}}}{H_{opt}^{0.75}} \cdot \frac{o}{j}$$

Assumed Hydraulic efficiency

$Q_{ref} = 1 \ [m^3/s]$

$a = 1$

$$m = 0.08 \cdot a \cdot \left[\frac{Q_{ref}}{Q_{opt}}\right]^{0.15} \cdot \left[\frac{45}{N_q}\right]^{0.06}$$

$$\eta_{hyd} = 1 - 0.055 \cdot \left[\frac{Q_{ref}}{Q_{opt}}\right]^{m} - 0.2 \cdot \left[0.26 - \textbf{log}\left[\frac{N_q}{25}\right]\right]^2 \cdot \left[\frac{Q_{ref}}{Q_{opt}}\right]^{0.1}$$

Impeller flow rate

$a_{sp} = 0.15$

$m_{sp} = 0.6$

$z_h = 1$ *Without balance holes*

$$Q_{sp} = Q_{opt} \cdot a_{sp} \cdot \frac{z_h}{N_q^{m_{sp}}}$$ *leakage flow rate through seal at impeller inlet*

$Q_e = 0$ *flow rate through axial thrust balancing device*

$$Q_{la} = Q_{opt} + Q_{sp} + Q_e$$

Volumetric efficiency

$$\eta_{vol} = \frac{Q_{opt}}{Q_{la}}$$

Shaft Dia

$$\tau_{shear} = 450 \ [MPa] \cdot \left| 1000000 \cdot \frac{Pa}{MPa} \right|$$ *Shear Strength of Stainless Steel (X20Cr13) 1.4021*

$$FOS = 1.8$$

$$\tau_{al} = \frac{\tau_{shear}}{FOS}$$

$$P_{max} = \rho \cdot g \cdot H_{opt} \cdot \frac{Q_{opt}}{\eta_{hyd}}$$

$$p = 1 \ [1/s]$$ **For unit conversion**

$$\omega = 2 \cdot \pi \cdot N \cdot \frac{p}{60}$$

$$d_w = \left[\frac{16 \cdot P_{max}}{\pi \cdot \omega \cdot \tau_{al}} \right]^{(1/3)}$$

Head Coefficient

$$f_t = 1.1$$

$$N_{q,ref} = 100$$

$$Si_{opt} = 1.21 \cdot f_t \cdot \mathbf{exp}\left[-0.77 \cdot \frac{N_q}{N_{q,ref}} \right]$$

Impeller Outlet Dia

$$d_2 = \frac{2}{\omega} \cdot \sqrt{2 \cdot g \cdot \frac{H_{opt}}{Si_{opt}}}$$

Number of blades

$$z_{la} = 5$$

Blade thickness

$$e_1 = 0.018 \cdot d_2$$ *Leading edge*

$$e_2 = \frac{e_1}{2}$$ *Trailing edge*

Impeller Inlet Dia for minimum relative velocity

$$f_{d1} = 1.14$$

$\lambda_r = 1$ *Swirl number*

$d_n = d_w + 0.005$ [m] *Hub Dia*

$$\phi_n = \frac{d_n}{d_2}$$

$$\phi_1 = f_{d1} \cdot \left[\sqrt{\phi_n^{\,2} + 0.00148 \cdot Si_{opt} \cdot \frac{N_q^{\,1.33}}{(\eta_{vol} \cdot \lambda_r)^{0.67}}} \right]$$

$$\phi_1 = \frac{d_{1o}}{d_2}$$

Impeller inlet dia for inner streamline

$d_{1i} = d_n + 0.006$ [m]

Table 3.1: Velocity triangle at Impeller inlet

$$d_{1b} = \frac{d_{1o} + d_{1i}}{2}$$ *Arithematic average of diameters*

$$d_{1m} = \sqrt{\frac{d_{1o}^{\,2} + d_{1i}^{\,2}}{2}}$$ *Geometric average of diameters*

$$A_1 = \pi \cdot \left[\frac{d_{1o}^{\,2} - d_{1i}^{\,2}}{4} \right]$$

$$A_1 = \pi \cdot d_{1b} \cdot b_1$$

$$c_{1m} = \frac{Q_{la}}{f_q \cdot A_1}$$ *Meridional component of absolute velocity*

$$c_{1u} = \frac{c_{1m}}{\tan(\alpha_1)}$$ *Circumferential component of absolute velocity*

Outer Streamline

$v = 1$ [1/s] **For unit conversion**

$$u_{1o} = \pi \cdot d_{1o} \cdot N \cdot \frac{v}{60}$$ *Circumferential Speed*

$$w_{1o} = \sqrt{c_{1m}^{\,2} + (u_{1o} - c_{1u})^2}$$ *Relative velocity*

$$\phi_1 = \frac{c_{1m}}{u_{1o}}$$ *Flow coefficient*

$$\beta_{1o} = \arctan\left[\frac{c_{1m}}{u_{1o} - c_{1u}} \right]$$ *Flow angle without blockage*

$i_1 = 4$ [Degree] *Incidence*

$\beta_{1b,o} = \beta_{1o} + i_1$

$\lambda_{1o} = 85$ [Degree] *Effect of inclination (twisted blades)*

$$\tau_{1,o} = \left[1 - \frac{z_{la} \cdot e_1}{\pi \cdot d_{1o} \cdot \sin(\beta_{1b,o}) \cdot \sin(\lambda_{1o})}\right]^{-1}$$ *Blade blockage at inlet*

$$\beta'_{1_o} = \arctan\left[c_{1m} \cdot \left[\frac{\tau_{1,o}}{u_{1o} - c_{1u}}\right]\right]$$ *Flow angle with blockage*

$$i_1 = \beta_{1b,o} - \beta'_{1_o}$$

Mean Streamline

$$u_{1m} = \pi \cdot d_{1m} \cdot N \cdot \frac{v}{60}$$

$$w_{1m} = \sqrt{c_{1m}^2 + (u_{1m} - c_{1u})^2}$$

$$\beta_{1m} = \arctan\left[\frac{c_{1m}}{u_{1m} - c_{1u}}\right]$$

$$\beta_{1b,m} = \beta'_{1_m} + i_1$$

$\lambda_{1m} = 87$ [Degree]

$$\tau_{1,m} = \left[1 - \frac{z_{la} \cdot e_1}{\pi \cdot d_{1m} \cdot \sin(\beta_{1b,m}) \cdot \sin(\lambda_{1m})}\right]^{-1}$$

$$\beta'_{1_m} = \arctan\left[c_{1m} \cdot \left[\frac{\tau_{1,m}}{u_{1m} - c_{1u}}\right]\right]$$

Inner Streamline

$$u_{1i} = \pi \cdot d_{1i} \cdot N \cdot \frac{v}{60}$$

$$w_{1i} = \sqrt{c_{1m}^2 + (u_{1i} - c_{1u})^2}$$

$$\beta_{1i} = \arctan\left[\frac{c_{1m}}{u_{1i} - c_{1u}}\right]$$

$$\beta_{1b,i} = \beta'_{1_i} + i_1$$

$\lambda_{1i} = 90$ [Degree] *No twist at inner streamline*

$$\tau_{1,i} = \left[1 - \frac{z_{la} \cdot e_1}{\pi \cdot d_{1i} \cdot \sin(\beta_{1b,i}) \cdot \sin(\lambda_{1i})}\right]^{-1}$$

$$\beta'_{1_i} = \arctan\left[c_{1m} \cdot \left[\frac{\tau_{1,i}}{u_{1i} - c_{1u}}\right]\right]$$

Outlet blade width

$$b_{2} = 0.017 + 0.262 \cdot \frac{N_q}{N_{q,ref}} - 0.08 \cdot \left[\frac{N_q}{N_{q,ref}}\right]^2 + 0.0093 \cdot \left[\frac{N_q}{N_{q,ref}}\right]^3$$

$$b_{2} = \frac{b_2}{d_2}$$

Table 3.2: Outlet velocity triangle

$$u_2 = \pi \cdot d_2 \cdot N \cdot \frac{v}{60}$$

$$A_2 = \pi \cdot d_2 \cdot b_2$$

$$c_{2m} = \frac{Q_{la}}{f_q \cdot A_2}$$

$$\phi_2 = \frac{c_{2m}}{u_2}$$

$$\lambda_2 = 90 \quad \text{[Degree]}$$

$$\tau_2 = \left[1 - \frac{z_{la} \cdot e_2}{\pi \cdot d_2 \cdot \mathbf{sin}\left(\beta_{2b}\right) \cdot \mathbf{sin}\left(\lambda_2\right)}\right]^{-1} \quad \textit{Blade blockage at outlet}$$

Outlet Angle Beta is calculated on basis of slip factor

$$\varepsilon_{lim} = \mathbf{exp}\left[-8.16 \cdot \frac{\mathbf{sin}\left(\beta_{2b}\right)}{z_{la}}\right]$$

$$f_1 = 0.98$$

$$d_{1m}' = \frac{d_{1m}}{d_2}$$

$$k_w = \mathbf{factor}\left(d_{1m}', \varepsilon_{lim}\right)$$

$$\gamma = f_1 \cdot k_w \cdot \left[1 - \frac{\sqrt{\mathbf{sin}\left(\beta_{2b}\right)}}{z_{la}^{0.7}}\right] \quad \textit{Slip factor}$$

$$H_{opt} = \eta_{hyd} \cdot \frac{u_2^2}{g} \cdot \left[\gamma - \frac{Q_{la}}{f_q \cdot A_2 \cdot u_2 \cdot \mathbf{tan}\left(\beta_{2b}\right)} \cdot \left[\tau_2 + A_2 \cdot d_{1m}' \cdot \frac{\mathbf{tan}\left(\beta_{2b}\right)}{A_1 \cdot \mathbf{tan}\left(\alpha_1\right)}\right]\right]$$

$$c_{2u} = u_2 \cdot \left[\gamma - c_{2m} \cdot \frac{\tau_2}{u_2 \cdot \mathbf{tan}\left(\beta_{2b}\right)}\right]$$

$$c_2 = \sqrt{c_{2m}^2 + c_{2u}^2}$$

$$w_{2u} = u_2 - c_{2u}$$

$$w_2 = \sqrt{c_{2m}^2 + w_{2u}^2}$$

$$\alpha_2 = \arctan\left[\frac{c_{2m}}{c_{2u}}\right]$$ *Absolute outlet angle without blockage*

$$\beta'_2 = \arctan\left[c_{2m} \cdot \frac{\tau_2}{w_{2u}}\right]$$ *Relative outlet angle with blockage*

$$\beta_2 = \arctan\left[\frac{c_{2m}}{w_{2u}}\right]$$ *Relative outlet angle without blockage*

$$\dot{\lambda} = \beta_{2b} - \beta'_2$$

$$\lambda = \beta_{2b} - \beta_2$$ *Deviation angle*

Blade Loading

$$\bar{w}_1 = \frac{w_{1o}}{u_2}$$

$$\bar{w}_2 = \frac{w_2}{u_2}$$

$$\xi_{eff} = 2 \cdot \pi \cdot \frac{Si_{opt}}{\eta_{hyd} \cdot z_{la} \cdot \dot{L} \cdot (\bar{w}_1 + \bar{w}_2)}$$

$$\xi_{al} = \left[\frac{40}{N_q}\right]^{0.77}$$

$$\xi_{eff} = 0.12 \cdot \xi_{al}$$

$$\dot{L} = \frac{L_{sch}}{d_2}$$

Throat Area

$$w_{1q} = 0.8 \cdot w_{1m}$$

$$A_{1q} = \frac{Q_{la}}{f_q \cdot z_{la} \cdot w_{1q}}$$

$$A_{1q} = a_{1t} \cdot b_1$$

Blade distance at outlet

$$t_2 = \pi \cdot \frac{d_2}{z_{la}}$$ *pitch*

$$\sin(\beta_{a2}) = 0.8 \cdot \sin(\beta_{2b})$$

$$\sin(\beta_{a2}) = \frac{a_{2o}}{t_2}$$

Table 3.6: Frictional Losses of rotating disk

$$R = \frac{d_2}{2}$$

$$Re = \rho \cdot u_2 \cdot \frac{R}{\mu}$$

$$d_{sp} = 0.48 \cdot d_2$$

$$r_{sp} = \frac{d_{sp}}{2}$$

$$\varepsilon = 0.15 \ [cm] \cdot \left| 0.01 \cdot \frac{m}{cm} \right| \quad \textit{Roughness of Galvanized Cast iron}$$

$$a_f = 1$$

$$s_{ax} = 0.02 \cdot d_2 \quad \textit{Sidewall gap}$$

$$\phi_{sp} = \frac{Q_{sp}}{\pi \cdot R^2 \cdot u_2} \quad \textit{Flow coefficient in impeller sidewall gap}$$

$$f_R = \left[\frac{\log\left[\frac{12.5}{Re}\right]}{\log\left[0.2 \cdot \frac{\varepsilon}{R} + \frac{12.5}{Re}\right]} \right]^{2.15} \quad \textit{Influence of roughness of rotating disk}$$

$$f_L = \exp\left[-350 \cdot \phi_{sp} \cdot \left[\left[\frac{R}{r_{sp}} \right]^{a_f} - 1 \right] \right] \quad \textit{Influence of leakage}$$

$$t_{ax} = s_{ax}$$

$$r_w = R$$

$$R_n = \frac{d_n}{2}$$

$$k_o = \frac{1}{1 + \left[\frac{r_w}{R}\right]^2 \cdot \left[\sqrt{\frac{r_w + 5 \cdot t_{ax}}{R}}\right]}$$

$$k_{RR} = \pi \cdot \frac{R}{2 \cdot Re \cdot s_{ax}} + 0.0625 \cdot (1 - k_o)^{1.75} \cdot f_R \cdot \frac{f_L}{Re^{0.2}} \quad \textit{Disk friction coefficient}$$

$$lamda = 15 \ [Degree]$$

$$P_{RR} = k_{RR} \cdot \rho \cdot \omega^3 \cdot \frac{R^5}{\cos(lamda)} \cdot \left[1 - \left[\frac{R_n}{R} \right]^5 \right] \quad \textit{Friction power per side of rotating disk}$$

Table 3.8(1): Hydraulic losses in Impeller

$$w_{av} = \frac{2 \cdot Q_{la}}{f_q \cdot z_{la} \cdot (a_{2o} \cdot b_2 + A_{1q})} \quad \textit{Average relative velocity in impeller channel}$$

$$Re_{imp} = \rho \cdot w_{av} \cdot \frac{L_{sch}}{\mu}$$

$$c_f = \frac{0.136}{\left[-\log\left[0.2 \cdot \frac{\varepsilon}{L_{sch}} + \frac{12.5}{Re_{imp}} \right] \right]^{2.15}}$$ *Friction coefficient*

$$D_h = 2 \cdot \left[\frac{a_{2o} \cdot b_2 + A_{1q}}{a_{1t} + b_1 + a_{2o} + b_2} \right]$$ *Hydraulic diameter*

$$c_d = (c_f + 0.0015) \cdot \left[1.1 + 4 \cdot \frac{b_2}{d_2} \right]$$ *Dissipation coefficient*

$$2 \cdot g \cdot \frac{Z_{la,R}}{u_2^{\,2}} = 4 \cdot c_d \cdot \frac{L_{sch}}{D_h} \cdot \left[\frac{w_{av}}{u_2} \right]^2$$ *Friction and mixing losses*

$$2 \cdot g \cdot \frac{Z_{la,C}}{u_2^{\,2}} = 0.3 \cdot \left[\frac{w_{1m} - w_{1q}}{u_2} \right]^2$$ *Shock loss at impeller inlet*

$$Z_{imp} = Z_{la,R} + Z_{la,C}$$ *Impeller loss*

Table 3.7(1): Leakage Losses through annular seal

$$d_{ref} = 100 \ [mm] \cdot \left| 0.001 \cdot \frac{m}{mm} \right|$$

$$2 \cdot \frac{s}{d_{sp}} = 0.004 \cdot \left[\frac{d_{ref}}{d_{sp}} \right]^{0.53}$$ *Radial Seal clearance*

$$L_{sp} = 0.13 \cdot d_{sp}$$ *Seal length*

$$H_p = \frac{u_2^{\,2} - u_{1o}^{\,2} + w_{1o}^{\,2} - w_2^{\,2}}{2 \cdot g} - Z_{imp}$$ *Static pressure rise in impeller*

$$y_{sp} = Re^{0.3} \cdot s \cdot \frac{d_{sp}}{d_2^{\,2}} \cdot \sqrt{\frac{s}{L_{sp}}}$$

$$k_{rot,i} = 0.9 \cdot y_{sp}^{\,0.087}$$ *Rotation factor for radially inward flow*

$$\delta_{H,sp} = H_p - k_{rot,i}^{\,2} \cdot \frac{u_2^{\,2}}{2 \cdot g} \cdot \left[1 - \frac{d_{sp}^{\,2}}{d_2^{\,2}} \right]$$ *Pressure difference across seal*

$$\zeta_{ea} = 1.1$$ *Inlet+Outlet loss*

$$\zeta_k = 1.1$$ *Loss per chamber*

Combine Reynolds Numbers due to circumferential and axial velocity in sidewall gap

$$u_{sp} = \pi \cdot d_{sp} \cdot N \cdot \frac{v}{60}$$

$$Re_u = 2 \cdot s \cdot u_{sp} \cdot \frac{\rho}{\mu}$$

$$Re_a = 2 \cdot s \cdot c_{ax} \cdot \frac{\rho}{\mu}$$

$$Re_c = \sqrt{Re_a^2 + \frac{Re_u^2}{4}}$$

$f = 0.03$ **Fig.3.14 Friction coefficient of Plain seal**

$e = 1$ [m] **For unit conversion**

$$c_{ax} = \sqrt{\frac{2 \cdot g \cdot \delta_{H,sp}}{\zeta_{ea} + f \cdot \frac{L_{sp}}{2 \cdot s} + \zeta_k \cdot \left[\frac{d_{sp}}{e}\right]^2 \cdot \left[\frac{s}{e}\right]^2}}$$ *Axial velocity in sidewall gap*

$$Q_{sp,i} = \pi \cdot d_{sp} \cdot s \cdot c_{ax}$$

$$\eta_h = \frac{H_{opt}}{H_{opt} + Z_{imp}}$$ *Efficiency after including all flow losses*

SOLUTION

Unit Settings: SI C kPa kJ mass deg

$a = 1$
$\alpha_2 = 13.6$ [Degree]
$A_{1q} = 0.001699$ [m^2]
$A_2 = 0.02158$ [m^2]
$a_f = 1$
$\beta_{1b,i} = 80.13$ [Degree]
$\beta_{1b,o} = 29.83$ [Degree]
$\beta_{1m} = 33.97$ [Degree]
$\beta_{1,dot,i} = 76.13$ [Degree]
$\beta_{1,dot,o} = 28.78$ [Degree]
$\beta_{2b} = 35.86$ [Degree]
$\beta_{a2} = 27.95$ [Degree]
$b_2 = 0.02643$ [m]
$c_{1m} = 4.648$ [m/s]
$c_2 = 11.14$ [m/s]
$c_{2u} = 10.83$ [m/s]
$c_d = 0.01291$
$\delta_{H,sp} = 5.087$ [m]
$d_{1i} = 0.02267$ [m]
$d_{1m,dot} = 0.3496$
$d_{1,dot} = 0.4866$
$D_h = 0.03967$ [m]
$d_{n,dot} = 0.06414$
$d_{sp} = 0.1248$ [m]
$e = 1$ [m]
$\varepsilon_{lim} = 0.3844$
$\eta_{hyd} = 0.9184$
$e_1 = 0.004678$ [m]
$f = 0.03$
$f_1 = 0.98$
$f_L = 0.7042$

$\alpha_1 = 90$ [Degree]
$A_1 = 0.01216$ [m^2]
$a_{1t} = 0.03273$ [m]
$a_{2o} = 0.07654$ [m]
$a_{sp} = 0.15$
$\beta_{1b,m} = 0.4014$ [Degree]
$\beta_{1i} = 69.68$ [Degree]
$\beta_{1o} = 25.83$ [Degree]
$\beta_{1,dot,m} = -3.599$ [Degree]
$\beta_2 = 16.39$ [Degree]
$\beta_{2,dot} = 16.78$ [Degree]
$b_1 = 0.05191$ [m]
$b_{2,dot} = 0.1017$
$c_{1u} = -2.008E-07$ [m/s]
$c_{2m} = 2.619$ [m/s]
$c_{ax} = 6.741$ [m/s]
$c_f = 0.007069$
$d_{1b} = 0.07458$ [m]
$d_{1m} = 0.09087$ [m]
$d_{1o} = 0.1265$ [m]
$d_2 = 0.2599$ [m]
$d_n = 0.01667$ [m]
$d_{ref} = 0.1$ [m]
$d_w = 0.01167$ [m]
$\varepsilon = 0.0015$ [m]
$\eta_h = 0.7482$
$\eta_{vol} = 0.9829$
$e_2 = 0.002339$ [m]
FOS = 1.8
$f_{d1} = 1.14$
$f_q = 1$

f_R = 4.509
g = 9.81 [m/s^2]
H_{opt} = 20 [m]
i_1 = 4 [Degree]
j = 1 [m$^{0.75}$]
$k_{rot,i}$ = 0.5568
k_w = 1
λ_{1i} = 90 [Degree]
λ_{1o} = 85 [Degree]
$\dot{\lambda}$ = 19.08 [degree]
lamda = 15 [Degree]
L_{sch} = 2.732 [m]
m = 0.1251
m_{sp} = 0.6
N_q = 36.14
o = 1 [s$^{0.5}$]
p = 1 [1/s]
ϕ_2 = 0.1327
P_{max} = 11847 [W]
Q_e = 0 [m^3/s]
Q_{opt} = 0.05556 [m^3/s]
Q_{sp} = 0.0009684 [m^3/s]
R = 0.13 [m]
Re_a = 2982
Re_{imp} = 1.654E+07
ρ = 998.2 [kg/m^3]
r_{sp} = 0.06238 [m]
s = 0.0002219 [m]
s_{ax} = 0.005198 [m]
$\tau_{1,m}$ = -0.09335
τ_2 = 1.025
τ_{shear} = 4.500E+08 [Pa]
t_{ax} = 0.005198 [m]
u_{1m} = 6.899 [m/s]
u_2 = 19.73 [m/s]
v = 1 [1/s]
w_{1m} = 8.318 [m/s]
w_{1q} = 6.655 [m/s]
w_2 = 9.284 [m/s]
$w_{2,dot}$ = 0.4705
ξ_{al} = 1.081
y_{sp} = 0.004008
ζ_k = 1.1
Z_{imp} = 6.732 [m]
$Z_{la,C}$ = 0.04232 [m]

f_t = 1.1
γ = 0.7369
H_p = 9.823 [m]
$i_{1,dot}$ = 1.049 [Degree]
k_o = 0.4772
k_{RR} = 0.003351
λ = 19.47 [degree]
λ_{1m} = 87 [Degree]
λ_2 = 90 [Degree]
λ_r = 1
$\dot{L}$ = 10.51
L_{sp} = 0.01622 [m]
μ = 0.001002 [N-s/m^2]
N = 1450
$N_{q,ref}$ = 100
ω = 151.8 [1/s]
ϕ_1 = 0.484
ϕ_{sp} = 0.0009249
P_{RR} = 449.5 [W]
Q_{la} = 0.05652 [m^3/s]
Q_{ref} = 1 [m^3/s]
$Q_{sp,i}$ = 0.0005864 [m^3/s]
Re = 2.556E+06
Re_c = 3644
Re_u = 4190
R_n = 0.008335 [m]
r_w = 0.13 [m]
Si_{opt} = 1.008
$\tau_{1,i}$ = 1.5
$\tau_{1,o}$ = 1.135
τ_{al} = 2.500E+08 [Pa]
t_2 = 0.1633 [m]
u_{1i} = 1.721 [m/s]
u_{1o} = 9.603 [m/s]
u_{sp} = 9.472 [m/s]
w_{1i} = 4.956 [m/s]
w_{1o} = 10.67 [m/s]
$w_{1,dot}$ = 0.5406
w_{2u} = 8.907 [m/s]
w_{av} = 6.076 [m/s]
ξ_{eff} = 0.1298
ζ_{ea} = 1.1
z_h = 1
z_{la} = 5
$Z_{la,R}$ = 6.69 [m]

No unit problems were detected.

Numerical Analysis of Flow Phenomena in a Centrifugal Pump Impeller of Low Specific Speed

Muhammad Ali [a, *], Adeel Javed [a]
[a] Center for Advanced Studies in Energy
National University of Sciences and Technology Islamabad, Pakistan
*Author. Email: 17teeali@uspcase.nust.edu.pk

***Abstract*— This paper aims to provide a numerical method approach to centrifugal pump manufacturers in Pakistan. Nowadays Computational fluid dynamics (CFD) is widely used to investigate the flow through turbomachines. In this research, centrifugal pump impeller of low specific speed ($N_q = 10.5$) is numerically investigated to study the flow phenomena and achieve better hydraulic performance through parametric analysis. The shear stress transport (SST) turbulence model is employed to solve 3-D steady RANS equations using CFD solver CFX (ANSYS). The volute hydraulic losses are calculated by loss coefficients predicted by Gulich [1] using Engineering Equation Solver (EES) program. The CFD results show the trend validated with the test data. Two design parameters blade wrap angle and outlet blade angle are considered as design parameter which greatly affect the hydraulic performance (head and efficiency). Additionally, a three-dimensional Rayleigh-Plesset model is also applied to investigate the cavitation (two-phase) flow inside the pump. The inlet blade angle is chosen as a design parameter to resist the cavitating flow inside the pump.**

Keywords*— Centrifugal pump, specific speed, numerical methods, design parameters, cavitation

I. INTRODUCTION

Centrifugal pumps are commonly used in industrial applications, domestic and irrigation, consuming large amount of electrical energy. Therefore, extensive research has been done to improve the optimized design of centrifugal pumps which greatly contributes to energy conservation.

The first approach for the optimization design is to use traditional one-dimensional design theory and now it has been advanced to three-dimensional design method. Inverse design method proposed by Gulich [1] is widely use by pump designers which gives the optimal geometry of the pump by defining the design conditions i.e. flow rate, head, and rpm. Another approach is to optimally combine design variables like blade angles, meridional shape etc. Xu et al. [2] in his research used CFD tools to find the combination of design parameters by orthogonal method for optimal design of the impeller. Yuan et al. [3] investigated the flow instabilities caused by cavitation through experimental means. Donmez et al. [4] presented how cavitation can be resisted by varying inlet blade angles on both hub and shroud. Tan et al. [5] studied the effect of wrap angle on head and efficiency of centrifugal pump and verified it with experimental work. Outlet blade angles and wrap angle are significant parameters in optimization design of impeller [6,7]. Kim et al. [8] reduced the flow recirculation and cavitation using multiple design variables such as meridional profile and incidence angles.

Computational fluid dynamics (CFD) has successfully contributed to the prediction of flow through turbomachines and helps in improvement of their design with significantly low cost and less time. Unfortunately, domestic pump manufacturers in Pakistan are not using this methodology to design centrifugal pump. This project aims to provide them the methodology for optimization design of centrifugal pump which will ultimately improve the pump performance and saves electrical energy. Impeller being the integral component of centrifugal pump that transfers the mechanical energy into hydraulic energy is selected in this research work for optimization. Firstly, the impeller is simulated at given flow rates to get the performance curves and then optimized design of impeller is proposed by varying the design parameters.

The low specific speed single-stage volute type centrifugal pump is selected for this research project. All the geometric parameters of the pump were provided by Golden Pumps. The important step is to choose the design parameters for optimization. The model pump impeller blades were in cylindrical form (untwisted blades) i.e. the shape of the blade is defined by a circular arc. Therefore, blade angles at hub and shroud and meridional shape could not be varied. According to Euler's turbomachine equation, the theoretical head of centrifugal pump is defined by

$$H_{th} = \frac{1}{g}(u_2 c_{\theta 2} - u_1 c_{\theta 1}) \qquad (1)$$

where $c_{\theta 2}$ and $c_{\theta 1}$ are circumferential velocity components of the fluid at impeller outlet and inlet respectively which are linked with blade angles. With fixed impeller diameter and rpm, the outlet blade angle has great impact on the head of pump. Therefore, outlet blade angle is chosen as optimization design parameter. The blade wrap angle is also selected as design parameter which controls the flow path. Cavitation is an important phenomenon to study in centrifugal pumps which causes flow disturbance due to vapor cavities inside the pump. Intense cavitation can lead to material erosion and produces noise and vibrations when the vapor filled ones (bubbles) implodes on the material surface. In terms of improvement in cavitation performance, the inlet blade angle is considered as design parameter as it directly influences the inlet flow conditions.

II. PROBLEM STATEMENT

A. Centrifugal Pump Model

For simplicity, the fluid flow through the impeller is investigated by numerical methods and flow losses inside the volute are calculated by the 1-dimensional loss model predicted by Gulich [1]. The detailed geometric parameters of the pump impeller are given in Table 1. The impeller geometry is drawn in Blade-Gen ANSYS by defining the meridional blade shape, blade angles and thickness.

Specific speed is used to classify impellers based on their performance regardless of size and speed at which it operates.

$$N_q = \frac{3.65N\sqrt{Q}}{H^{3/4}} \qquad (2)$$

Table 1. Geometric parameters of the test pump

Description	*Parameter*	*Value*
Design flow rate	$Q/(m^3.h^{-1})$	3.6
Head	$H/(m)$	18
Rotation speed	$N/(rev.min^{-1})$	2900
Specific speed	N_q	10.5
Number of blades	Z	6
Impeller inlet diameter	$D_1/(mm)$	42
Impeller outlet diameter	$D_1/(mm)$	130
Inlet blade angle	$\beta_1/(°)$	26
Outlet blade angle	$\beta_2/(°)$	36.5
Blade wrap angle	$\varphi/(°)$	82

B. Numerical Method

Numerical calculations are done using the CFD program CFX (ANSYS) to solve 3-D steady Reynolds-Averaged Navier-Stokes (RANS) equations. The SST (shear stress transport) turbulence model is adopted which employs k-ω model close to the wall surface and k-ε model in the passage flow. The impeller blade and wall surfaces are subject to no-slip boundary conditions. Water at standard ambient conditions (25°C) is used as a working fluid. Due to the rotational periodicity, single passage of the impeller is modeled to avoid the more computational time requirements. The inlet boundary condition is defined by total pressure and mass flow rate is used at the outlet.

C. Cavitation Model

The two-phase (vapor-liquid) flow occur inside the pump when the fluid's static pressure falls below its saturation pressure. The model established on Rayleigh-Plesset equation is used to examine the cavitating flow. This model executed in CFX involves the nuclei radius which is assumed to be 1μm. The two-phase flow is modeled as a homogeneous mixture having the same flow conditions. At inflow condition, vapor volume fraction is assigned a zero value because vapors will generate within the impeller as cavitation starts. The total pressure is lowered step-by-step at inlet while keeping mass flow rate fixed at the outlet.

Net positive suction head *(NPSH)* is the difference between total pressure head at the pump inlet and the vapor pressure head of the fluid.

$$NPSH = \frac{P_{in}}{\rho g} + \frac{{v_{in}}^2}{2g} - \frac{P_v}{\rho g} \qquad (3)$$

where P_{in} and v_{in} are absolute pressure and velocity at pump inlet respectively; ρ is the density and P_v is the vapor pressure (P_v=3574 Pa at 25°C) of the fluid. The $NPSH_3$ is accepted as a criterion of cavitation when the head drops by 3% of the actual head developing without cavitation.

D. Computational Domain and Mesh

The structured mesh (hexahedral) elements of the impeller are generated in Turbo-Grid shown in Figure 1. The mesh is carefully refined to satisfy the requirement of y^+value. The y^+below 1 is maintained at the wall surface of blade, hub, and shroud to investigate flow in viscous sublayer. The mesh elements effect the CFD results, that's why grid independence test is carried out. Five meshes of impeller are created varying from coarse to the finer grid. As the mesh reaches 1,20,000 elements, the head does not change significantly as shown in Figure 2. Therefore, 1,20,000 mesh elements for a single passage is chosen in numerical simulations of the model impeller.

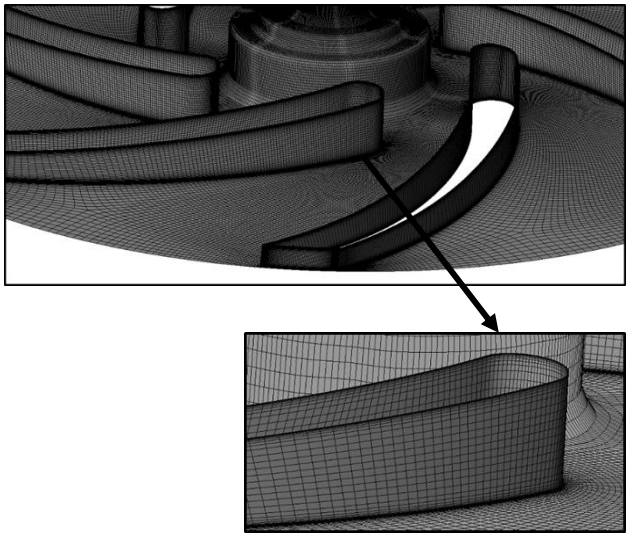

Figure 1. Structured mesh of impeller with refined leading edge

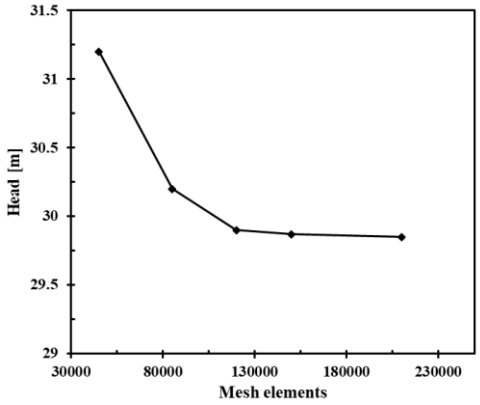

Figure 2. Mesh independence test

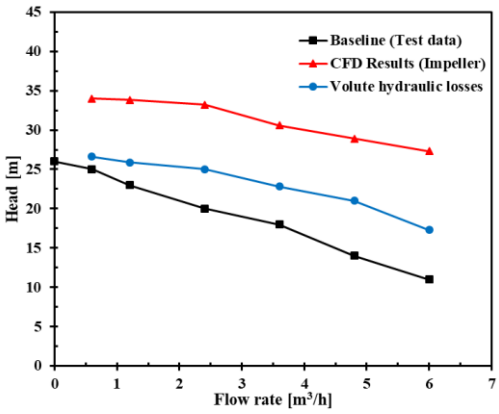

Figure 3. Pump performance curves (Q-H curves)

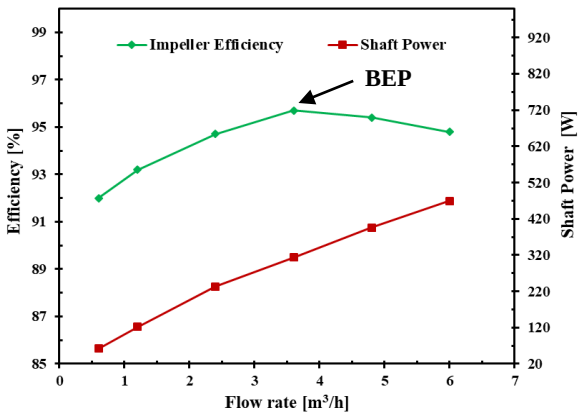

Figure 4. Hydraulic efficiency and shaft power

III. VOLUTE LOSS MODEL

The fluid's kinetic energy is converted into static pressure when flow exits from the volute. The spiral volute of model pump has a rectangular cross-section with a radial type diffuser at the exit.

The hydraulic losses inside the volute are calculated through the 1-dimensional prediction model presented by Gulich [1]. The calculations are done using Engineering Equation Solver (EES) programming.

The coefficient for the volute loss is given as:

$$\xi_{vol} = \xi_F + \xi_S + \xi_{Dc} + \xi_D \tag{4}$$

The volute loss coefficient consists of the coefficient for the losses by friction, shock, deceleration and in the diffuser.

The coefficient for the friction loss is given as:

$$\xi_F = \frac{Q}{{u_2}^2}\left(c_f + 0.0015\right)c^3\Delta A \tag{5}$$

where ΔA is the wetted surface.

The coefficient for shock loss is given as:

$$\xi_S = {\varphi_{2,imp}}^2\left(\tau_2 - \frac{b_2}{b_3}\right)^2 \tag{6}$$

The coefficient for deceleration loss is given as:

$$\xi_{Dc} = a + b\frac{c_{3q}}{c_2} + c\left(\frac{c_{3q}}{c_2}\right)^2 \tag{7}$$

The coefficient for diffuser loss is given as:

$$\xi_D = \frac{{c_x}^2}{{u_2}^2}\left(1 - c_p - \frac{1}{{A_R}^2}\right) \tag{8}$$

Total head loss in the volute is

$$H_{loss} = \frac{\xi_{vol} \times u_2^2}{2g} \tag{9}$$

where $u_2$is the circumferential speed at the impeller outlet.

IV. NUMERICAL RESULTS AND DISCUSSION

Centrifugal pump performance is described by plotting the head at various flow rates. A characteristics curve includes its hydraulic efficiency and shaft power, both of which are plotted against the various flow rate as shown in Figure 3 and Figure 4.

$$H = \frac{P_{tot_{outlet}} - P_{tot_{inlet}}}{\rho_{water} \times g} \tag{10}$$

$$\eta_{hyd} = \frac{\rho g Q H_{tot}}{T.\omega} \tag{11}$$

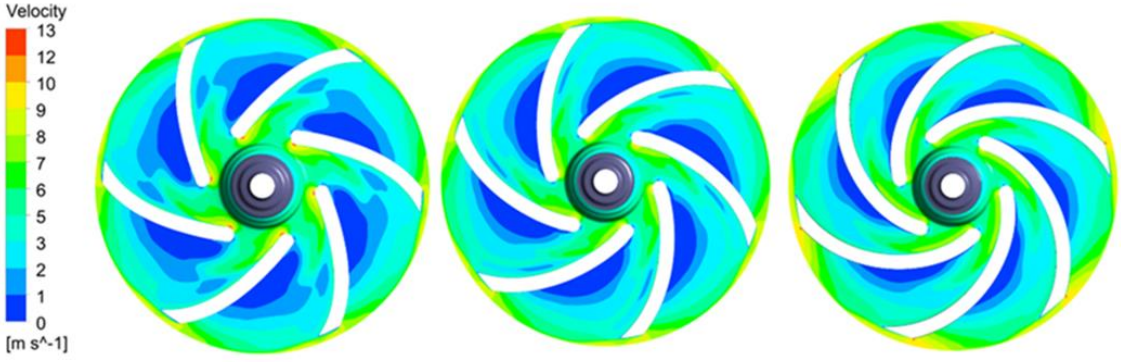

a) Wrap 65° b) Wrap 82° c) Wrap 110°

Figure 5. Relative velocity contours on mid-span section of the impeller with varying wrap angle

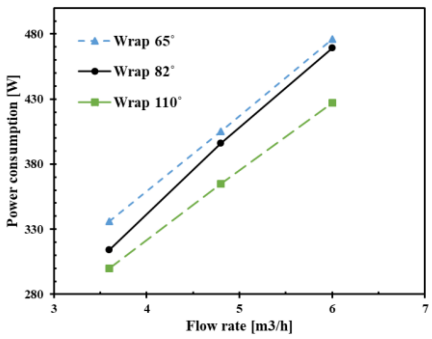

Figure 6. Shaft power consumption with varying wrap angle

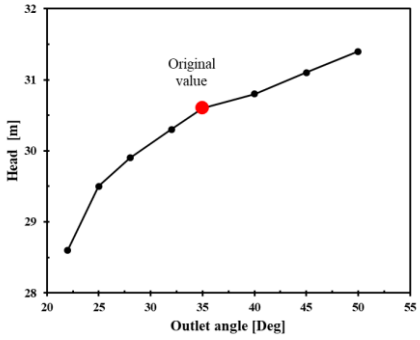

Figure 7. Head curve with varying outlet blade angle

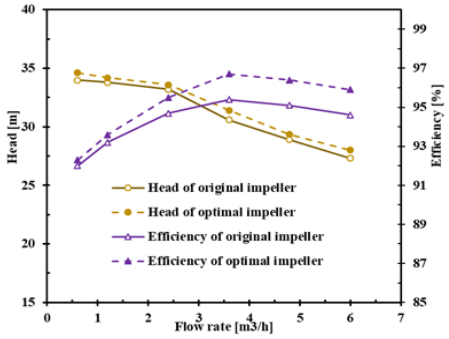

Figure 8. Comparison of original and optimal impeller

The combined results of CFD and volute loss model shows that the pump head is close to the test data (baseline) at low flow rates (part-load operation). The main reason for high error in the values at higher flow rates is the shaft power requirement. According to Golden Pumps data, the pump is driven by 0.5 hp (370 W) induction motor. Figure 4 shows that at BEP (best efficiency point) and above, power requirement increases from 315 W to 470 W, therefore, the predicted head is higher than baseline head. Also, the impeller sidewall gaps are not included in the computational domain in which flow leakage occurs that further produces the head loss. But the results follow the trend of baseline at design and off-design conditions which can be a good approximation to optimize the impeller.

A. Effect of Blade Wrap Angle

The angle made by the tangent lines on leading and trailing edge of the blade defines the blade wrap angle. The wrap angle is varied from 65º to 110º. A large wrap angle offers controlled flow in the impeller by reducing the secondary losses (flow separation). But as the wrap angle increases, the fluid has to undergo long flow path and produce more friction losses. A small wrap angle generates short flow path with less frictional losses, but the flow distribution is not uniform and higher secondary losses will occur. The relative velocity contours on mid-span location of the impeller with different wrap angles are shown in Figure 5. In terms of hydraulic performance, the impeller with wrap angle 110º offers relatively higher efficiency by reducing the shaft power consumption with marginal loss in the head (due to higher frictional losses). The shaft power consumption at higher flow rates is shown in Figure 6.

B. Effect of Outlet Blade Angle

The outlet blade angle is varied from 22º to 50º to get its impact on head and efficiency of the pump. The impeller with wrap angle of 110º has been simulated with varying outlet blade angle. With increase of outlet blade angle, head continuously increases as shown in Figure 7. It can be seen from velocity triangle at impeller outlet in Figure 9, that $c_{\theta 2}$ is higher with large outlet angle which is transferred to the fluid in the form of head. The impeller with wrap angle of 110º and outlet angle of 50º is the optimal one. The head and efficiency improvement of the original and optimal impeller is shown in Figure 8.

C. Effect of Inlet Blade Angle on Cavitating flow

The development of cavitation is simulated only at design flow condition. For better cavitation performance, $NPSH_3$ must be small. The static pressure contours on mid-span of the impeller without cavitation are shown in Figure 10. When the static pressure falls below the saturation pressure of the fluid, vapor cavities start growing at various cross sections of the blades with different size and intensity.

Initially, the head drop curve at inlet blade angle of 26º is drawn which shows sudden head drop when lowering the inlet pressure reaches a certain level. The $NPSH_3$ of original pump is 2.78 m. The inlet blade angle which directly influences the cavitation phenomenon is decreased

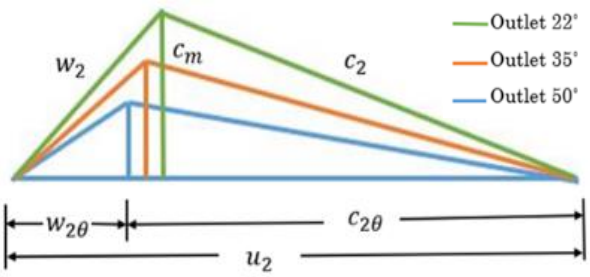

Figure 9. Velocity triangle at impeller exit for different outlet angles

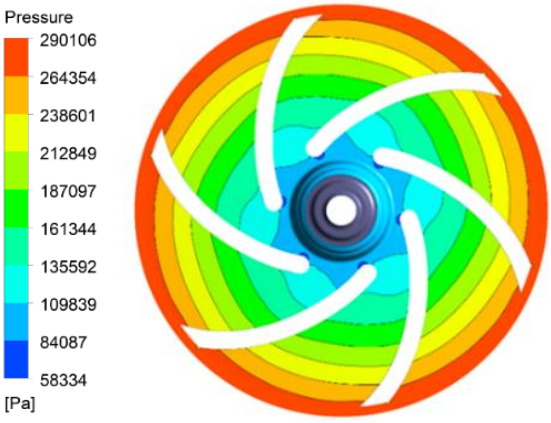

Figure 10. Static pressure contours on mid-span of impeller

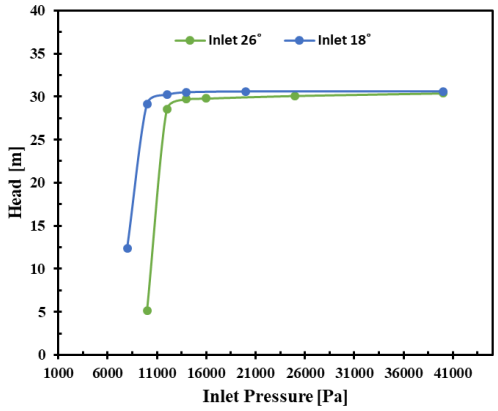

Figure 11. Head drop curves with varying inlet angles

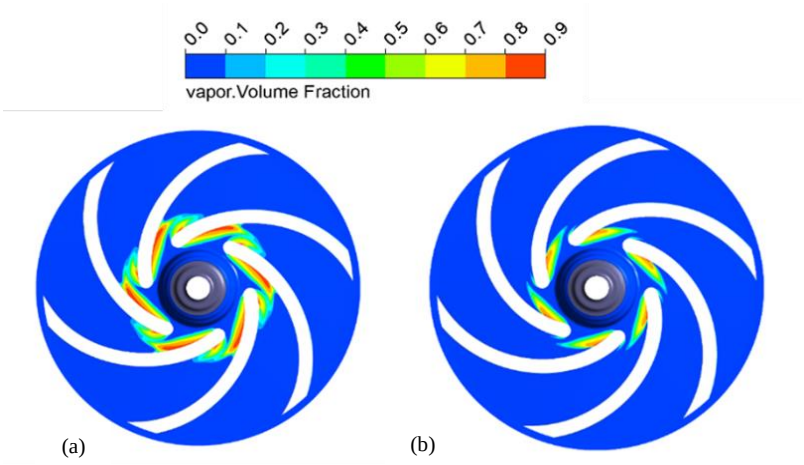

Figure 12. Vapor volume fraction with (a) Inlet angle 26º (b) Inlet angle 18º

from 26º to 18º and it showed positive effect on cavitation resistance. The head drop curves with decreasing inlet blade angle is compared in Figure 11. The $NPSH_3$ of 1.66 m for the optimal pump is achieved with inlet blade angle of 18º.

For inlet total pressure equal to 20,000, 16,000, 12000Pa, thin vapor cavities start to develop at the suction side of blade near the leading edge. When lowering the total inlet pressure to 10,000Pa, the long and thick cavities develop that disturbs the flow in impeller. The optimal pump impeller shows a strong resistance towards cavitation as shown in Figure 12.

V. CONCLUSIONS

This research work analyzes the flow pattern in the centrifugal pump impeller and its effect on the performance. This study gives the parametric analysis of certain design variables to achieve better hydraulic performance. The impeller with wrap angle of 110º consumes the least shaft power while the outlet blade angle of 50º gives the maximum head. The optimal impeller gives an improvement in hydraulic efficiency of 1.6% rise as compared to original impeller. The cavitation performance is also improved by decreasing inlet blade angle. The inlet blade angle of 18º gives $NPSH_3$ of 0.82 m decline as compared to original pump.

Some of the recommendations for future work are to include other pump components like volute and impeller sidewall gaps in the computational domain for more accurate results. The stall condition at part-load operation is an important aspect to study that greatly impairs the pump performance. The unsteady flow in the volute causes flow distortion in the impeller as well. The volute curvature and cutwater design also have great influence on hydraulic performance of the centrifugal pump. The investigation of radial and axial thrust acting on the impeller is vital for appropriate sizing of shaft and bearings.

ACKNOWLEDGMENT

The author(s) would like to recognize the support of Golden Pumps Private Limited, Gujaranwala Pakistan and U.S. Pakistan Center for Advanced in Energy, National University of Sciences and Technology (USPCAS-E NUST) in completing this research work.

REFERENCES

[1] J. F. Gülich, *Centrifugal Pumps*. 2013.

[2] Y. Xu, L. Tan, S. Cao, and W. Qu, "Multiparameter and multiobjective optimization design of centrifugal pump based on orthogonal method," *Proc. Inst. Mech. Eng. Part C J. Mech. Eng. Sci.*, vol. 231, no. 14, pp. 2569–2579, 2017.

[3] Y. Fu *et al.*, "Numerical and experimental analysis of flow phenomena in a centrifugal pump operating under low flow rates," *J. Fluids Eng. Trans. ASME*, vol. 137, no. 1, 2015.

[4] A. H. Dönmez, Z. Yumurtaci, and L. Kavurmacioglu, "The effect of inlet blade angle variation on cavitation performance of a centrifugal pump: A parametric study," *J. Fluids Eng. Trans. ASME*, vol. 141, no. 2, 2018.

[5] L. Tan, B. Zhu, S. Cao, H. Bing, and Y. Wang, "Influence of blade wrap angle on centrifugal pump performance by numerical and experimental study," *Chinese J. Mech. Eng. (English Ed.*, vol. 27, no. 1, pp. 171–177, 2014.

[6] X. Han, Y. Kang, D. Li, and W. Zhao, "Impeller optimized design of the centrifugal pump: A numerical and experimental investigation," *Energies*, vol. 11, no. 6, 2018.

[7] J. Pei, W. Wang, S. Yuan, and J. Zhang, "Optimization on the impeller of a low-specific-speed centrifugal pump for hydraulic performance improvement," *Chinese J. Mech. Eng. (English Ed.*, vol. 29, no. 5, pp. 992–1002, 2016.

[8] H.-S. Shim, K.-Y. Kim, and Y.-S. Choi, "Three-Objective Optimization of a Centrifugal Pump to Reduce Flow Recirculation and Cavitation," *J. Fluids Eng.*, vol. 140, no. September, 2018.